STRUCTURAL DESIGN OPTIMIZATION OF A PEDIATRIC STENT FOR PULMONARY ARTERY STENOSIS

Lalla Zineb Idrissi, McGill University, Montreal

August 2009

A thesis submitted to McGill University in partial fulfillment of the requirements of the degree of Masters of Engineering

In loving memory of my mom,
To my dad,

Acknowledgments

The author wishes to express her gratitude to her supervisor, Dr. Rosaire Mongrain not only for his invaluable support, advice and guidance but also for his kindness, understanding and patience throughout the hard times. His devotion to his work and field helped the author stay focused and motivated towards finishing the degree but also to appreciate the field of cardiovascular mechanics. Special thanks go to Drs. Olivier Bertrand and Josep Rodés (*Centre hospitalier de l'université Laval*) for their time and answers to numerous questions. The author is also thankful to all graduate friends and colleagues for their invaluable assistance. The author would also like to convey thanks to the National Research Council of Canada and Baylis Medical Company for providing the financial means to complete this project.

Lastly, my deepest love and gratitude to my parents: my late mother for her endless love, her being there at every step of the way and believing in me and my father who encouraged, supported and had confidence in me.

Abstract

Congenital cardiovascular defects occur in approximately one percent of live births annually. One example is pulmonary artery stenosis, a narrowing of the major artery connecting the right ventricle to the lungs. As a result, the blood flow towards the lungs is decreased, making it difficult for blood to be reoxygenated.

In order to remedy such a condition, pediatric cardiologists often opt for a minimally invasive procedure that is, inserting a stent, a tubular prosthetic to hold the artery open. However, the available stents that are inserted in the infant are adult stents designed for coronary artery disease. These adult stents do not accommodate for growth in children, therefore re-dilations of the implanted stent are required every three years or so. However, as the child is growing, open heart surgery has to eventually be performed to remove this no longer adequate prosthesis.

The goal of this project is to optimize a pediatric stent design the major characteristic of which is an open loop design that accommodates for the infant's artery growth. This design was generated following engineering design steps (problem definition, design embodiment, etc.) and is optimized through numerical simulations and mechanical testing.

After several iterations, the current generation of stents fulfills a majority of the design requirements On the other hand, this design is not without flaws or limitations, and it should be further improved. However, it is a promising design which could potentially be successful in animal experiments

Finally, a stent designed specifically for the pediatric population would be a major breakthrough in the field of pediatric cardiology as only minimally invasive surgeries would be performed and open heart surgery avoided.

Résumé

Annuellement, 1% de nouveaux nés souffrent de maladies cardiovasculaires congénitales. Parmi celles-ci, nous retrouvons la sténose de l'artère pulmonaire qui est, en fait, un rétrécissement du vaisseau acheminant le sang oxygéné des poumons vers le ventricule droit. L'utilisation d'un stent (ou tuteur) adulte habituellement employé pour traiter les sténoses des artères coronaires soulève un problème d'importance majeure. En effet, le stent coronarien, n'ayant pas le potentiel de s'adapter à la croissance somatique de l'enfant, il est alors nécessaire d'avoir recours à une chirurgie à cœur ouvert ultérieure pour enlever le stent lorsqu'il devient inadapté à la taille de l'artère. Une première génération de stents a pu être développée en suivant les différentes étapes couramment utilisées pour concevoir un nouveau *design* dans le domaine de l'ingénierie (Définition de la problématique, génération de concepts, etc.). A partir de là, la méthodologie suivie consiste à améliorer le design en ayant recours à des simulations numériques ainsi qu'à des tests mécaniques. Cela se fait de façon incrémentale dépendamment des résultats obtenus à l'étape précédente. Suivant la méthodologie décrite précédemment, il a été possible d'améliorer le design et diverses générations de stents ont pu êtres créées et améliorées.

La génération actuelle de stents répond à la majorité des exigences structurelles. Bien que ce design ne soit pas sans failles, ce serait un pas prometteur si les tests in vivo s'avéraient concluants et positifs.

Finalement, un stent pour la population pédiatrique pourrait constituer une importante percée dans le domaine de la cardiologie pédiatrique permettant ainsi d'avoir recours à des procédures non invasives, évitant une chirurgie à cœur ouvert.

Table of contents

List of Figures

List of tables

1. Clinical Background

In a biomedical engineering design project, one of the first key steps is to understand the complex physiological environments under which the medical device is to be used. Therefore, as a starting point, a brief synopsis of the functioning of the heart, the role of the pulmonary artery, the pulmonary artery stenosis (PAS) condition, its symptoms and treatments will be presented.

1.1. Heart anatomy and physiology

The heart is a hollow muscular organ located in the center of the chest. It has four chambers; the upper two chambers are the right and left atria, and the lower two chambers are the right and left ventricles.

The heart's vital function is to pump blood to the rest of the body. The average heart pumps about 7,200 liters of blood each day, and its different compartments do so in unidirectional flow. Heart valves play an important role in maintaining this unidirectional flow. In fact, with each heartbeat, pressure changes force the valves to open allowing the blood to flow and then close tightly to prevent the backflow of blood.

The right ventricle sends oxygen-poor blood through the pulmonary arteries (PA), to the lungs, where the blood is oxygenated and carbon dioxide removed. The left ventricle sends oxygen-rich blood through the aorta, to the rest of the body and the heart itself, delivering oxygen and other nutrients to tissues while gathering waste products and transferring them to other organs for proper disposal [1-3].

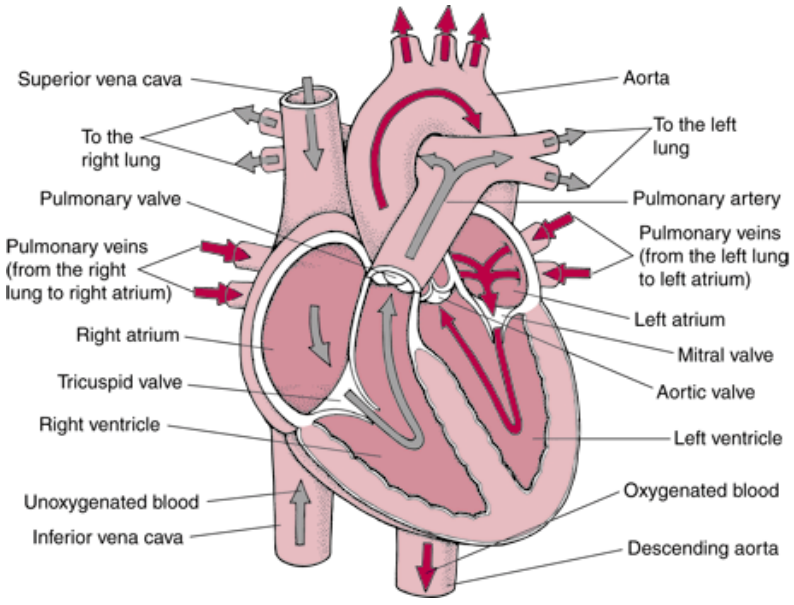

Figure 1.1: Blood flow through the heart

1.1.1 Arterial wall architecture

Arteries exhibit elasticity which contributes to move blood away from the heart to the body's organs. The architecture of the vessel wall comprises three layers: the *tunica intima*, the *tunica media* and the *tunica adventitia*.

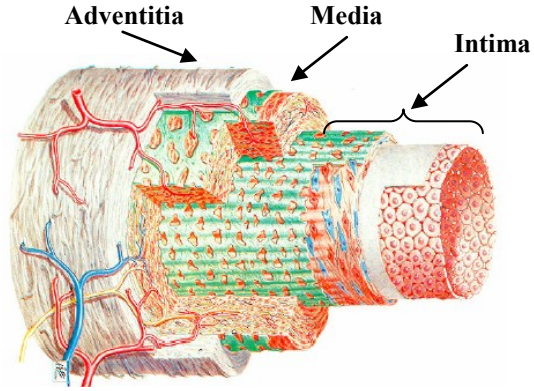

Figure 1.2: Arterial wall architecture. From [4]

The *tunica intima* is the inner layer of arteries; it is composed of an endothelial lining, separating blood flow from the other layers, a network of connective tissue and a layer of elastic fibres. The *tunica media* is the middle and thickest layer composed mainly of smooth muscle (for strength) and elastin arranged in roughly spiral layers. The outermost layer, the *tunica adventitia* is a strong covering composed mainly of collagen fibres to act as a support, connective tissue and elastic fibres [5].

1.2. Pulmonary artery stenosis

As shown in figure 1, the pulmonary artery plays a key role in the circulation. In fact, it is the conduit that brings oxygen-depleted blood from the right ventricle to the lungs for reoxygenation. It is composed of branches; the right PA conveys the blood to the right lung and the left PA to the left lung.

In about 1% of live births, a congenital defect occurs due to abnormal development of the fetal heart. One of the most frequent defect is pulmonary stenosis. Pulmonary stenosis can be subdivided into four types:

1. *Valvar pulmonary stenosis:* the valve leaflets are thickened and, or narrowed;
2. *Supravalvar pulomary stenosis:* the pulmonary artery just above the valve is narrowed resulting in decreased blood flow;
3. *Subvalvar (infundibular) pulmonary stenosis:* the muscle under the valve is thickened reducing the outflow from the right ventricle;

4. *Branch peripheral pulmonic stenosis*: The main, right or left pulmonary arteries are narrowed [6, 7].

In the present project, branch peripheral pulmonic stenosis is the type of interest as the goal here is to address the stenosis when it occurs in the artery and not the valve itself.

Peripheral pulmonary artery stenosis occurs in 2 to 3% of patients with congenital heart disease and it has several different etiologies (table 1.1) [8]. In fact, branch pulmonary artery stenosis can occur as congenital, that is as a "native" lesion (often referred to as primary). In such instances, the stenosis can occur as the only lesion (40% of the cases), or associated with other congenital cardiac defects (20% of the cases) including tetralogy of fallot, pulmoncary artery atresia with ventricular septal defect and truncus arteriosus. The stenosis can also occur as part of a generalized syndrome, with William-Beuren and Alagille syndromes being the most notable examples. Other syndromes include Keutel, Noonan and Rubella syndromes among others [9-11].

Pulmonary artery stenosis can also be "acquired" as a result from an attempted surgical repair in the area of the pulmonary artery or on the artery itself (often referred to as secondary). In fact, branch pulmonary arteries are very thin walled, low pressure vessels easily and frequently compressed by adjacent intrathoracic structures. In their *non-operated* state, these vessels are able to move away from the higher pressure structures. However, following surgery, the scarring in the area of the artery reduces its ability to move away from compression by adjacent structures, thus resulting in a stenosis. For example, patients with tetralogy of Fallot often require augmentation of the pulmonary flow; the surgically created shunts can cause narrowings of the pulmonary arteries, independently of any other existing PAS associated with the cardiac defect [12, 13].

Peripheral pulmonary artery stenosis etiology	Percentage
Isolated lesion	**Accounts for 40% of PAS cases**
Syndromes	**N/A**
Williams-Beuren syndrome	PAS occurs in 39-83% of Williams-Beuren syndrome cases
Alagille syndrome	PAS occurs in 70-85% of Alagille syndrome cases
Congenital heart defects	**Accounts for 20% of PAS cases**
Valvar pulmonary stenosis (VPS)	PAS occurs in 30% of this defect cases
Atrial spetal defect	PAS occurs in 15% of atrial septal defect cases
Ventricular spetal defect	PAS occurs in 15% of this defect cases
Tetralogy of Fallot	PAS occurs in 15% of this defect cases
Acquired	**N/A**
Post surgery	**N/A**

Table 1.1: Etiologies of peripheral pulmonary artery stenosis

As to its morphological forms, peripheral pulmonary artery stenosis is categorized into four types as shown in figure 1.3 below.

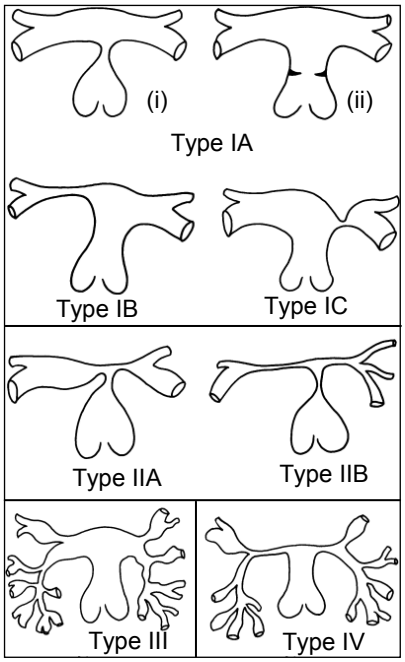

Figure 1.3 : A sketch of classification of peripheral pulmonary artery stenosis. From [8]

In type I, the lesion can occur as a single constriction in the main (IA), right (IB) or left (IC) pulmonary arteries, and can be the result of a membranous diaphragm within the vessel (IA-i) or the result of a constriction (IA-ii). Type II lesions can vary from short localized segment (IIA) to long segment stenoses (IIB) occuring at the pulmonary artery bifurcation, involving the distal end of the main PA and the origin of the right and left PA. In type III, stenosis occurs at multiple peripheral segments, with normal main and proximal branch pulmonary arteries. Finally, a type IV lesion involves multiple peripheral segments as well as the central pulmonary arteries [11].

Obstruction in branch pulmonary arteries causes severe hemodynamic effects and leads to various complications some of which are listed below: [9, 14, 15]

- The lung supplied by the narrowed vessel is under perfused which can cause a ventilation-perfusion mismatch;
- Pulmonary hypertension in the other branch of pulmonary arteries can induce pulmonary vascular disease;
- Over perfusion of the other lung can result in pulmonary oedema;
- The right ventricle must pump harder to try to move the blood through the narrowed passageway. This additional workload can result in right ventricular hypertension, dysfunction or even failure;

- Arrhythmia;
- Sudden death.

1.3. Current solutions: minimally invasive procedures

The most common treatment choices for PAS are interventional cardiac catheterization procedures[6], either balloon angioplasty or stent placement. Both of these procedures are termed minimally invasive procedures because smaller skin incisions are needed, resulting in minimal trauma as compared to an open surgical procedure.

1.3.1. Balloon angioplasty

Successful balloon angioplasty of pulmonary artery stenosis was initially described by Lock and colleagues in 1981 in lambs [16] and later in infants [17, 18].

During balloon angioplasty, a catheter, a small flexible tube, is inserted through the femoral vein (in the groin area) and guided to the stenosed location in the pulmonary artery (Figure 1.4). A small balloon, mounted on the tip of the catheter, is inflated slowly for 15 to 30 seconds once it reaches the narrowed vessel (Figure 1.5). Pressures used to inflate the balloon vary from 5 to 20 atm. Inflating the balloon opens up the blocked passageway. The balloon is then deflated and the catheter removed.

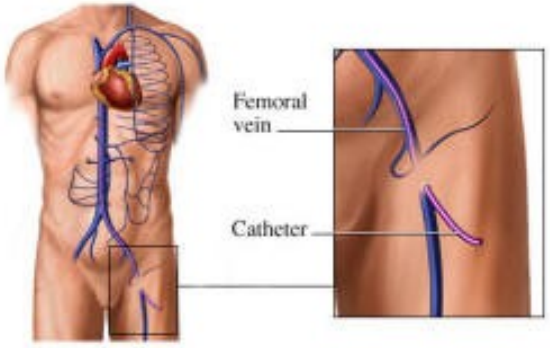

Figure 1.4: Catheter insertion in the femoral vein. From [19]

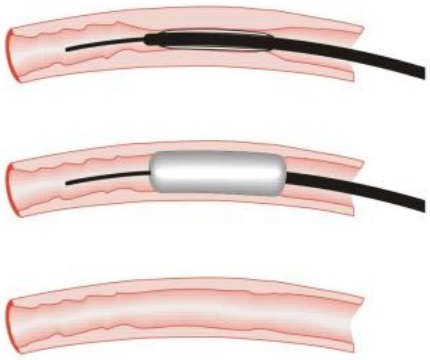

Figure 1.5: Percutaneous transluminal angioplasty. From [20]

Note that during balloon expansion, there is usually little effect on the overall hemodynamics by the fully inflated balloon and sufficient run off to other areas of the lungs [13].

Despite the promising early reports on balloon angioplasty outcomes [17, 18, 21, 22], early failures of balloon angioplasty can be seen because of elastic recoil of the vessel, fibrotic lesions that are too rigid to be dilated or external compression of the vessel wall. Later failures are associated with restenosis (reoccurrence of stenosis) of successfully dilated narrowings [23, 24].

1.3.2. Stenting

Intravascular stents are tubular metallic meshes (Figure 1.6) which, as opposed to balloon angioplasty, provide a basis to resist vessel elasticity and external compressive forces. The first stent for human use was introduced by Palmaz et al. in 1985 for use in adult iliac, biliary and renal stenoses [25-29]. Dr. Schatz later modified the stent for use in adult coronary artery stenosis [30].

This stent has then been used by Dr. Charles Mullins in 1988 in his experiments. In fact, he reported the first use of stents in pulmonary arteries and veins in a canine model [9]. From the same group, O'Laughlin et al. described their successful application in patients in 1991 [31]. Since then, the use of stents for treatment of congenital heart disease has expanded tremendously, with various reports of successful short and long term results [14, 24, 32-44].

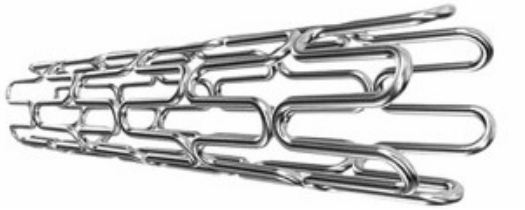

Figure 1.6: A stent – A tubular metallic support. From [45]

Stents can be classified as self expanding and as balloon expandable stents. Briefly, self-expanding stents are cut to the desired artery diameter and are then restrained within a covering sheath (Figure 1.7). Withdrawal of this membrane uncovers the stent which then assumes its original predetermined shape [15, 46, 47]. This type of stents will not be further discussed here as it has been shown that their use is limited in the pediatric population [48-50].

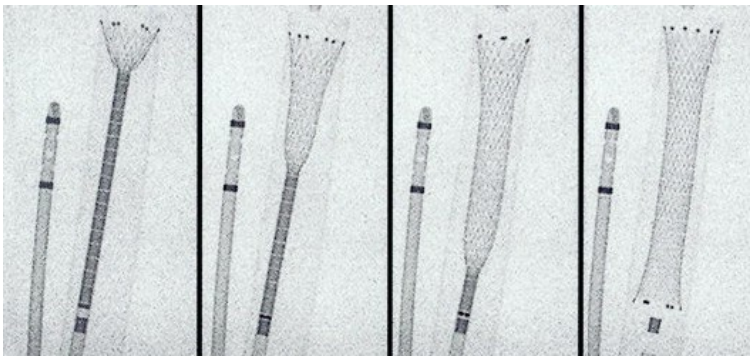

Figure 1.7: Deployment of a self-expanding stent. From [32]

Balloon expandable stents, on the other hand, are deployed using a balloon catheter and are commonly used for treating children [13, 32]. These will be discussed in greater detail in a later section.

The procedure for implanting a balloon expandable stent resembles the balloon angioplasty procedure in that a balloon catheter is used as well. Stenting however requires the insertion of a stent which is mounted on the deflated balloon. The stent is usually compressed or '*crimped*' onto the balloon; crimping tools can be used but no single tool is satisfactory for the multiple combinations of balloon and stent sizes therefore, manual crimping is often used [13].

The first step in the implantation procedure is to insert a guide wire through a small incision in the vein; a long sheath is then directed towards the narrowed region. The long sheath is used to prevent the prosthetic from catching on intravascular structures and getting displaced off the balloon while en route to the lesion. The sheath has two additional uses; in fact, it is essential in recovering a balloon in the event of puncture or rupture of the balloon during implantation. Moreover, the sheath allows for easy exchange between different sized balloons in the case of multiple stenoses or sequential dilations of a single stent.

Once the guide wire and the sheath are positioned, the balloon catheter with the mounted stent is inserted through the sheath and threaded in the vessel towards the stenosed location. Once in position, the balloon is inflated pushing the stent against the stenosed vessel wall, thus opening the narrowing. The balloon is then deflated and the catheter removed. With the balloon deflation, the stent remains expanded, providing structural support to the now dilated area (Figure 1.8).

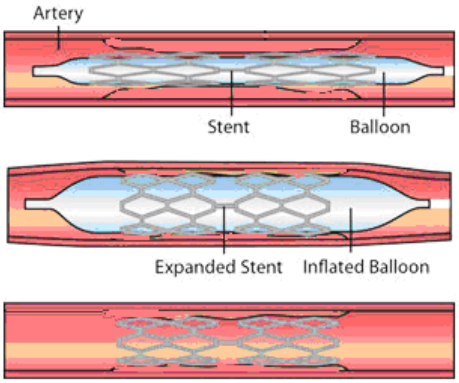

Figure 1.8: Illustration of the stent deployment. From [51]

It is worthy to note that when implanting a single stent, to branch pulmonary arteries, two venous accesses are used: one for the stent delivery and the other for monitoring angiography. The two femoral veins are usually the preferred access routes; however, in larger children, in the case of an obstructed femoral vein for example, an internal jugular vein and a femoral vein can be the two venous accesses during the procedure.

1.4. Indications and success criteria for stent catheterization procedures

As for any interventional procedure, patient indication is a key determinant of success. Potential candidates are patients with lesions that are not accessible to surgery or those who have already had surgery in the affected region and for which a catheterization procedure would avoid an additional traumatic open heart surgery [52, 53]. Moreover, since surgery on branch pulmonary artery stenosis is itself a cause of branch pulmonary artery stenosis (see section 1.2), and balloon dilation does not maintain the full patency of the vessel, the use of stents in pulmonary arteries is considered as the primary therapy for these vascular lesions.

More specifically, indications for a stent interventional procedure are one or more of the following: [10, 52]

- A right ventricular systolic pressure that is 75% or more, higher than the left ventricular pressure;
- Stenotic vessel diameter that is more than 50% smaller than that of the surrounding vessels, associated with decreased blood flow to the affected lung;
- Hypertension of other unobstructed pulmonary artery segments (Mean distal pressure greater than 25mm Hg).
- Clinical symptoms (e.g.: exercise intolerance or increasing cyanosis)

On the other hand, criteria for success are the following: [35, 52]

- Increase of more than 50% of the stenosed vessel diameter;
- Decrease of more than 20% of the ratio of right ventricular systolic pressure to aortic systolic pressure.
- Increase of more than 20% in flow to the stented lung by perfusion scan.

1.5. Complications associated with stent catheterization procedures

Although complications, both minor and major, associated with a stent catheterization procedure are numerous, they occur in rare instances (procedural success rates greater than 93%, [14, 34, 35, 37, 52]). Some of these complications are briefly discussed here.

- **Restenosis:** Restenosis is the result of a cascade of cellular and molecular events within the *injured* vascular wall. Three distinct processes contributing to restenosis can be discerned: elastic recoil, arterial remodelling and neotinimal hyperplasia. ***Elastic recoil*** occurs immediately after angioplasty and results in an immediate loss of lumen diameter; it is a

more pronounced phenomenon in balloon angioplasty than in stenting [54]. ***Arterial remodelling*** can be categorized as both positive and negative. Positive remodelling is a compensatory response that limits narrowing of the vessel; whereas negative remodelling is the opposite process and its underlying mechanisms are not completely understood [54, 55]. Finally, ***neointimal hyperplasia*** is a thickening of the intima following trauma. In fact, immediately after a metallic surface is in contact with the circulating blood, a series of biological events occur to colonize the stent with tissue. Endothelial denudation of the vessel wall results in the loss of antithrombotic factors and as a result, a thrombotic layer covers the stent. Within a few days to weeks, this layer is progressively replaced by fibromuscular tissue[56]. Within approximately six months, a 1-2 mm thin neointimal layer forms around the stent, embedding it in the vessel wall (Figure 1.9) [57, 58]. A greater degree of neointimal proliferation may however cause restenosis. Nevertheless, various reports describe restenosis due to intimal hyperplasia in young patients as a rare event (in about 1.5% of the cases) [47, 53, 59].

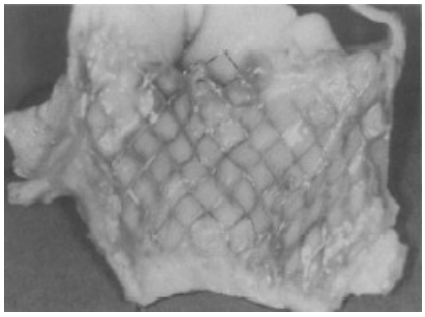

Figure 1.9 : An explanted stent from a pig pulmonary artery shows a thin membrane of neo-endothelial cells 3 months post implantation. From [12]

Note that it is not clear to which extent the first two stages (elastic recoil and vessel remodelling) contribute to restenosis. In contrast, in-stent restenosis is primarily a result of neointimal hyperplasia [55, 60].

- **Embolization:** Embolization, migration or malpositioning of the stent is a difficult complication as it might require urgent surgical retrieval of the stent. It has been shown, however, that this occurs in rare instances [34, 37, 47].

- **Stent fracture:** Stent fractures are a rare complication when implanted in pulmonary arteries [61]. However, O'Laughlin et al. reported one event which occurred in a right ventricular conduit[34]. This has been explained by the proximity of the stent to the beating myocardium. It appears that the prosthesis did not withstand the cyclic stresses and fractured.

As with any interventional procedure, various complications could occur. However, refinements in the stenting techniques and several technological advances resulted in an important decrease in complications associated with the implantation of stents in the pulmonary arteries [13, 62].

1.6. Children and stenting: The challenge

In addition to the indications for catheter interventional procedures listed earlier, one must keep in mind an additional indication that applies to stenting for the pediatric population. In fact, stent implantation in small children will result in an iatrogenic stenosis that is, as the child grows, the stent fixes the vessel diameter preventing the enlargement of its distal end (Figure 1.10). Unequivocally, a subsequent surgical procedure is performed to remove the stented segment of pulmonary artery. This is particularly the case if stents are implanted in major central pulmonary artery branches in young infants. Therefore, except in extremely extenuating, life-threatening circumstances, stents should not be used in small vessels that will eventually grow to be larger than the maximum possible diameter of the stent [13]. Stents, however, can be used temporarily for relieving stenosis in younger patients for which a future surgical intervention will be performed to alleviate another coexisting condition [36, 37].

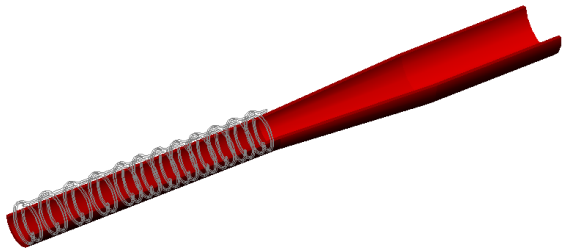

Figure 1.10: Schematic representation of iatrogenic stenosis

With the current available treatment options, possible candidates for stent implantation are therefore older children or young adults of sufficient vessel size for a large stent to be implanted which will be further dilated to near-adult vessel diameter when the need rises [12, 23, 53]. In this patient group, re-expansion of the stent is routinely performed to the maximal stent diameter, safely and effectively [23, 59, 63-65]. These stent redilations to accommodate for somatic growth have been successfully performed up to ten years after implantation [64].

Furthermore, even when used for older children with congenital heart defects, the stents are specifically designed for adults coronary indications, therefore various requirements specific to these young patients are not fulfilled by using regular adult coronary stents.

When used in children, adult stents are often overdilated to a diameter greater than the maximal diameter listed by the manufacturer and as a result what is called foreshortening of the stent occurs: as the stent is expanded in the radial direction, it is shortening along its

length. This results in an insufficient longitudinal coverage of the stenosis and serial implantation of stents might therefore be needed (Figure 1.11) [13, 66].

$$Foreshortening = \left(L_{initial} - L_{postdeployment} / L_{initial} \right) \times 100 \quad (1.1)$$

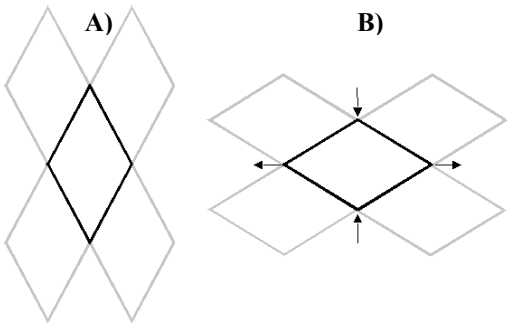

Figure 1.11: Illustration of foreshortening: A) Undeployed B) Deployed

Another limitation in using adult stents in children is that delivery mechanisms used to implant these stents are often too large for the small vessel diameters of children [59].

Finally, adult stents are often too rigid and render it difficult for the physician to easily pass them through the tortuous path and tight curves towards the pulmonary arteries.

1.6.1. Stents available to the pediatric cardiologist

Balloon expandable stents can be classified as small, medium, large and extra-large depending on the vessel diameter to be treated [32].

The stents listed below were approved for treatment of various lesions in the adult patient (iliac, renal, biliary and peripheral vessels) and were not specifically designed for infants and children (with the exception of the Numed CP stent). For each group of stents, the vessels treated in congenital lesions, descriptions of the stents, their advantages and drawbacks are given.

A) Small stents

Small stents have a maximum expanded diameter ranging from 3 to 6 mm. They are used in treating coronary arteries in adult patients and are rarely used for younger patients as their maximum possible diameter is too small. Therefore, this group of stents will not be discussed.

B) Medium stents

Medium stents can be expanded to maximum diameters of 10 to 12 mm. They are used in treatment of segmental and subsegmental branch pulmonary arteries, femoral and pulmonary veins, and Blalock-Taussig shunts. This group of stents includes the Palmaz 4 series (Johnson and Johnson Interventional Systems, Warren, NJ), the Palmaz Corinthian series (Johnson and Johnson Interventional Systems), the Bridge stent (Medtronic-AVE, Santa Rosa, CA) and Genesis stent (Johnson and Johnson- Cordis Corp., Miami Flakes, FL)

- **Palmaz 4 series**: As mentioned earlier, the Palmaz stent has been the first endovascular stent. Since its introduction, it has been used in treatment of congenital lesions for over a decade and a half [13]. The Palmaz 4 series or *renal* stents are laser cut in a biocompatible stainless steel tube (SS 316L); the resulting slots form seven cell rows which become diamond shaped after expansion. (Figure 1.12)

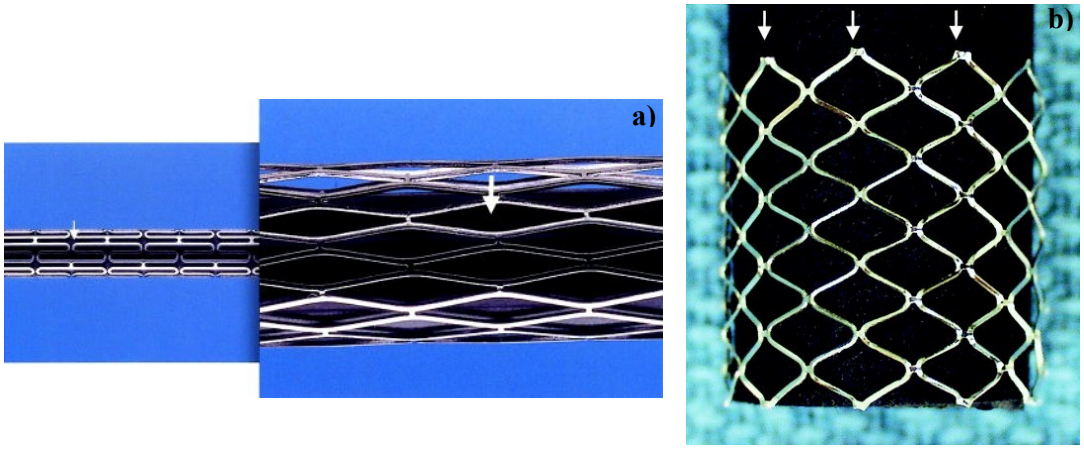

Figure 1.12 : Palmaz stent a) Deployed diamond shaped cells b) Sharp edges. From [32]

As its name indicates, the potential maximal diameter of the Palmaz 4 series stent is 4mm. However, one must note that this is the labeled maximal diameter for use in the adult biliary system, whereas in reality, for use in congenital lesions, the stent can be overdilated up to 10mm. This is performed not without drawbacks. In fact, as explained earlier, foreshortening occurs when overdilating the stent. Experiments have shown that when the stent is expanded to 9mm, it shortens by about 19-23%, and by 33-40% when expanded to 10mm.

Another disadvantage inherent to the Palmaz design is the rigidity of the stent making it difficult to negotiate the turns in the pediatric cardiovascular system. Moreover, the sharp edges increase the risk of balloon rupture and vessel trauma during expansion. On the other hand, the Palmaz 4 series provides good radial strength and has the advantage of a long history of use and thus greater experience among pediatric cardiologists. [13, 24, 32]

- **Palmaz Corinthian series**: The Palmaz Corinthian series is in fact a modified Palmaz stent designed for the adult biliary system with the goal of improving pre-deployment flexibility as compared to the original Palmaz. The design still consists of rows of seven cells laser, cut in a

stainless steel 316L tube, with the addition, however, of omega hinges between cells and smoother ends (Figure 1.13) [32, 67, 68]. The stent can be dilated to a greater maximum diameter than its predecessor (12mm as compared to 10mm for the Palmaz 4 series). However, foreshortening is similar in both stents. The Corinthian stent shortens by 24 to 26 % of its original size when expanded to 9mm, 38 to 41% at 10 mm and 35 to 60% at 12mm [32, 68]

As for its radial strength, it is comparable to that of the Palmaz 4 series. Therefore, its main advantage resides in its improved flexibility and rounded edges.

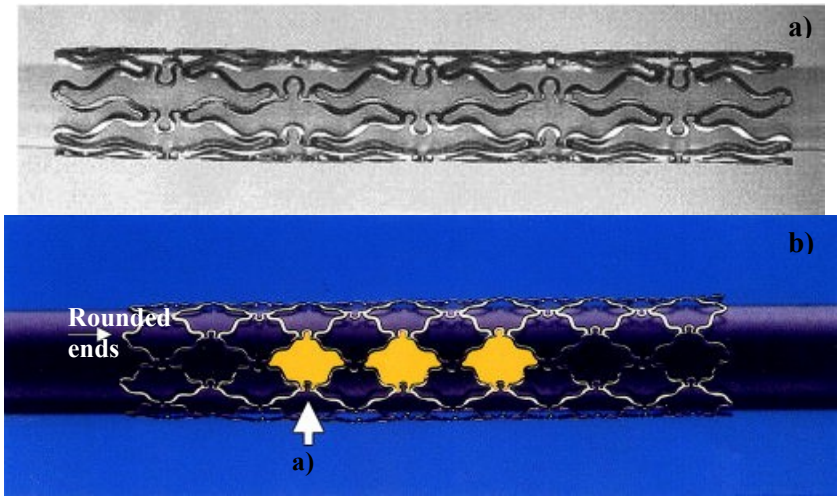

Figure 1.13: Palmaz Corinthian stent; a) crimped, b) deployed. From [32]

- **Bridge stent** is a biliary stent made of rows of stainless steel sinusoidal elements which are laser fused. (Figure 1.14) It can be dilated up to 14 mm in diameter without significant foreshortening (about 22%; less at smaller diameters – see table 1.2). However, poorer radial strength has been noted at large diameters (see Figure 1.17)

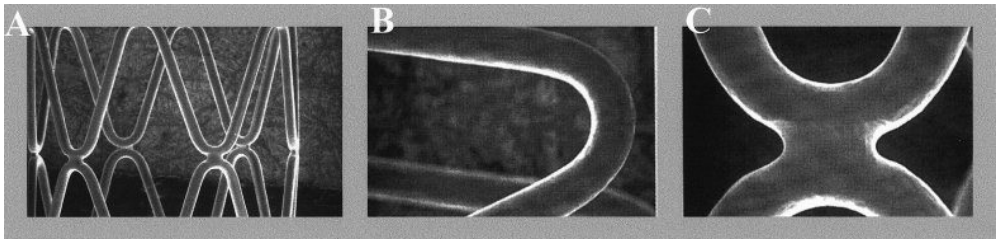

Figure 1.14 : Bridge stent – a) sinusoidal elements, b) smooth ends c) laser welds. From [32]

- **Genesis biliary stent** is similar to the Palmaz Corinthian stent with the difference of having 'omega' hinges between each row of diamond-shaped cells. (Figure 1.15) These sigmoidal hinges allow for greater flexibility, and prevent foreshortening as they elongate during expansion.

Figure 1.15: Genesis stent a) undeployed, b) deployed; note the elongated hinges (white arrow). From [32]

The Genesis stent can itself be categorized as *medium* and *large*. The maximum possible diameter is 10 mm and 12 mm for the medium and large genesis stent, respectively [13]. Limited data shows 11% foreshortening when expanded at 10mm, however further experimental data is not available at this time. The Genesis stent is expected to replace the earlier Palmaz 4 and Corinthian lines [69, 70].

Figures 1.16 and 1.17 below compare foreshortening data for some of the stents described above at various diameters.

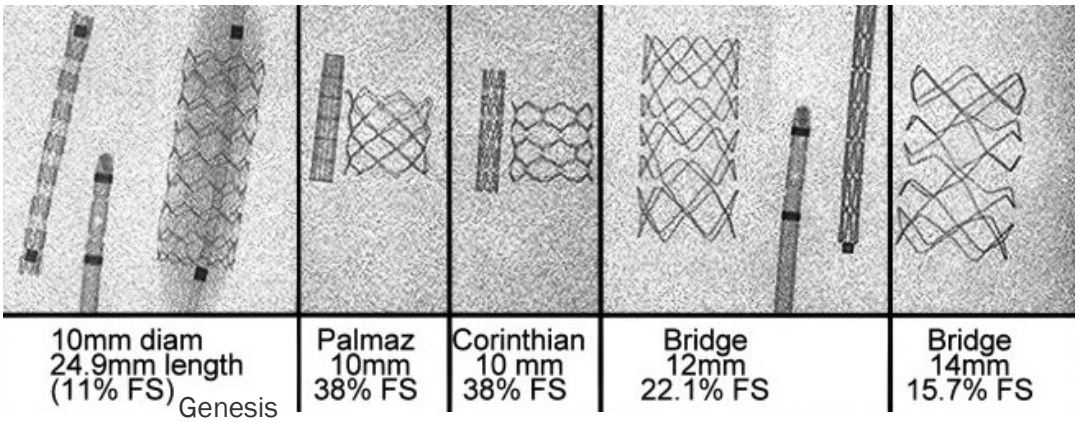

Figure 1.16 : Foreshortening comparison for medium stents under fluoroscopy. From [32]

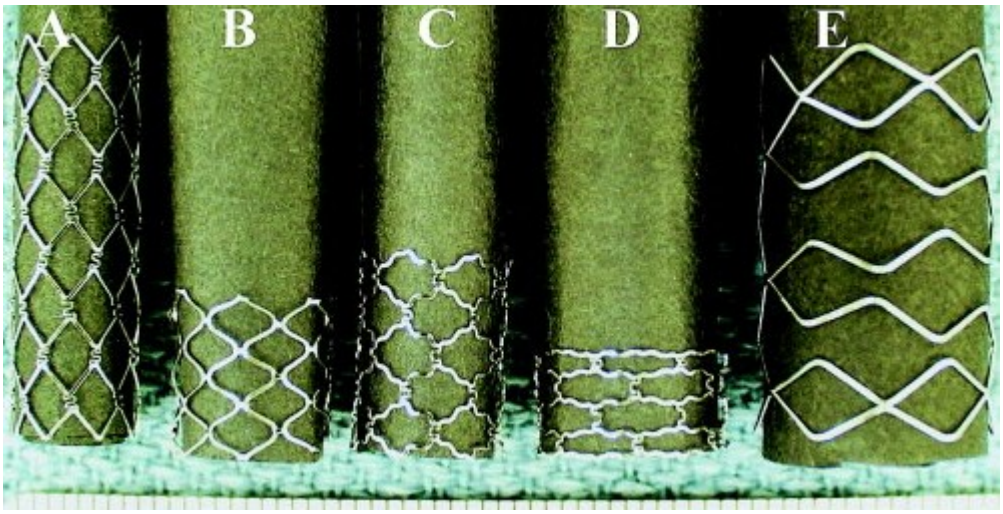

Figure 1.17: Foreshortening comparison for medium stents. A) Genesis at 8mm, B) Palmaz at 10mm, C) Corinthian at 10mm, D) Corinthian at 12mm, E) Bridge at 14mm. From [32]

Table 1.2 below summarizes some key characteristics of the stents described above as well as their principal advantages and disadvantages.

	Non expanded diameter	Rated diameter	Maximal diameter	Foreshortening		Available Lentghs	Sheath sizes	Advantages	Disadvantages
				%	At D				
Palmaz 4 series	2.5mm	4 mm	10 mm	19-23%	9mm	10 – 39mm	6-7 Fr*	• Long experience in pediatric cardiology • Good radial strength	• Sharp edges increase the risk of balloon rupture and vessel trauma during expansion • Rigid • Overdilation can cause -significant foreshortening
				33-40%	10mm				
Palmaz corinthian series	N/A	4-8 mm	11-13mm	24-26%	9mm	12 – 39mm	6-7Fr	• Improved flexibility (vs. Palmaz) • Good radial strength, comparable to that of the Palmaz 4 series • Rounded edges	• Significant foreshortening when expanded to its maximal diameter;
				38-41%	10mm				
				55-60%	12mm				

* 1French (Fr) is equivalent to 1/3mm.

	Non expanded diameter	Rated diameter	Maximal diameter	Foreshortening		Available Lentghs	Sheath sizes	Advantages	Disadvantages
Bridge Stent	N/A	6-10mm	14mm	3-15%	10mm	28-100 mm	7-8Fr	• Flexibility • Largest maximal diameter among medium sized stents • Least amount of foreshortening	• Weaker radial strength at 14mm. • Little experience among pediatric cardiologists
				15-18%	12mm				
				22%	14mm				
Genesis Stent (Medium, Large)	N/A	M: 7mm L: 9mm	M: 10mm L: 12mm	11%	10mm[†]	**M:** 12, 15, 18, 24mm **L:** 19,29, 39, 59, 79mm	6-7Fr	• Omega hinge prevents excessive foreshortening; • Flexibility; • Good radial strength as compared to Palmaz.	• Limited use in congenital lesions, • Little experience among pediatric cardiologists

Table 1.2 : Key characteristics of medium stents

[†] Data from 32. Ing, F., *Stents: what's available to the pediatric interventional cardiologist?* Catheter Cardiovasc Interv, 2002. **57**(3): p. 374-86.[30], not specified whether data is applicable to the medium or large genesis stent.

C) Large stents

Large stents can be expanded to maximum diameters of 18 mm. They are used in treatment of major central vessels: main and proximal branch pulmonary arteries, lobar branch pulmonary arteries, the superior and inferior vena cava, proximal iliac vein, aorta and Fontan baffles. This group of stents includes the Palmaz 8 series (Johnson and Johnson Interventional Systems, Warren, NJ), the DoubleStrut LD stent (Sulzer-IntraTherapeutics, St. Paul, MN), the Genesis XD (Johnson and Johnson- Cordis Corp., Miami Flakes, FL), the Mega LD (ev3, Plymouth, MN) and the Cheatham-Platinum (CP) six-zig stent (Numed, Hopkinton, NY).

- **Palmaz 8 series of stents**: As its name indicates, the Palmaz 8 series of stents are Palmaz stents with maximal *advertised* diameter of 8 mm. However, this stent can be dilated up to 18mm with 40%foreshortening and appropriate radial strength. It is similar to the Palmaz 4 series except that it has 10 cells per row.

- **DoubleStrut LD stent**: The intrastent doublestrut LD has been designed for the biliary tree. It consists of double rows of fine stainless steel struts for the inner rings and single rows for the outer rings (Figure 1.18) [71]. This design is termed an 'open-cell' design as cell geometry changes upon expansion with the three diamond shaped cells opening to become one single large cell (Figure 1.19-A). This 'open-cell' configuration and very thin struts contribute to the stent's flexibility while still providing good radial strength. It can be dilated to up to 18-20 mm. This can be done without significant foreshortening (less than 10%) when the stent is dilated serially, that is, for example, first expanding the stent on a 10-12mm balloon and then a second dilation on appropriate balloons to reach 15-18mm. As can be seen from figure 1.21B, serial dilation allows for gradual cell separation whereas in figure 1.21A where the stent has been deployed with a single large balloon, the cells do not separate and significant foreshortening is present. This is explained by a phenomenon called *dumbelling* or *dogboning*: the ends of the balloon expand first, almost completely, while the central portion is still undeployed (Figure 1.20) Moreover, as the ends deploy first, they tend to compress the center of the stent longitudinally preventing the cells from separating and thus the stent from elongating.

As for radial strength, it has been shown that the double strut LD provides less radial strength than Genesis XD (described below) and Palmaz 8 (At D>12mm) [70, 72].

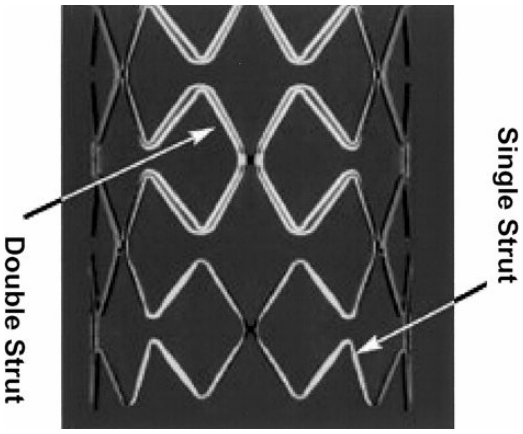

Figure 1.18: DoubleStrut LD stent

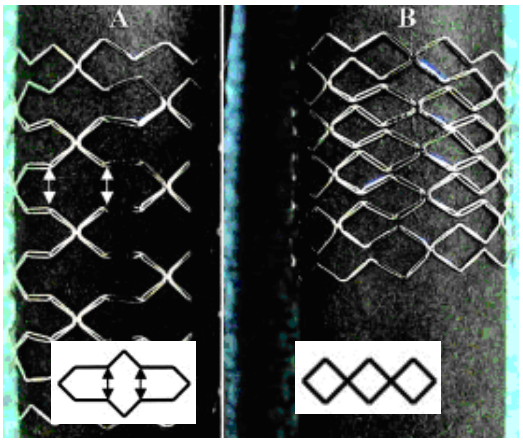

Figure 1.19: Double Strut LD A) Cell separation prevents foreshortening B) Undeployed stent. From [32]

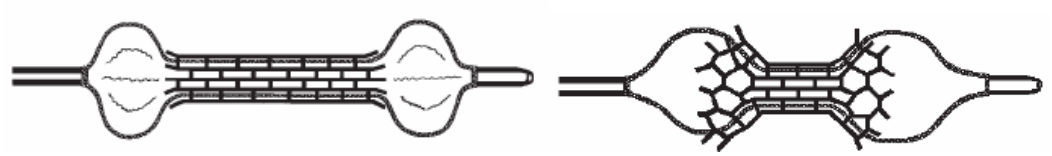

Figure 1.20: Schematic of dumbelling phenomenon: Only ends of the balloon expand at first compressing middle portion of the stent. From [13]

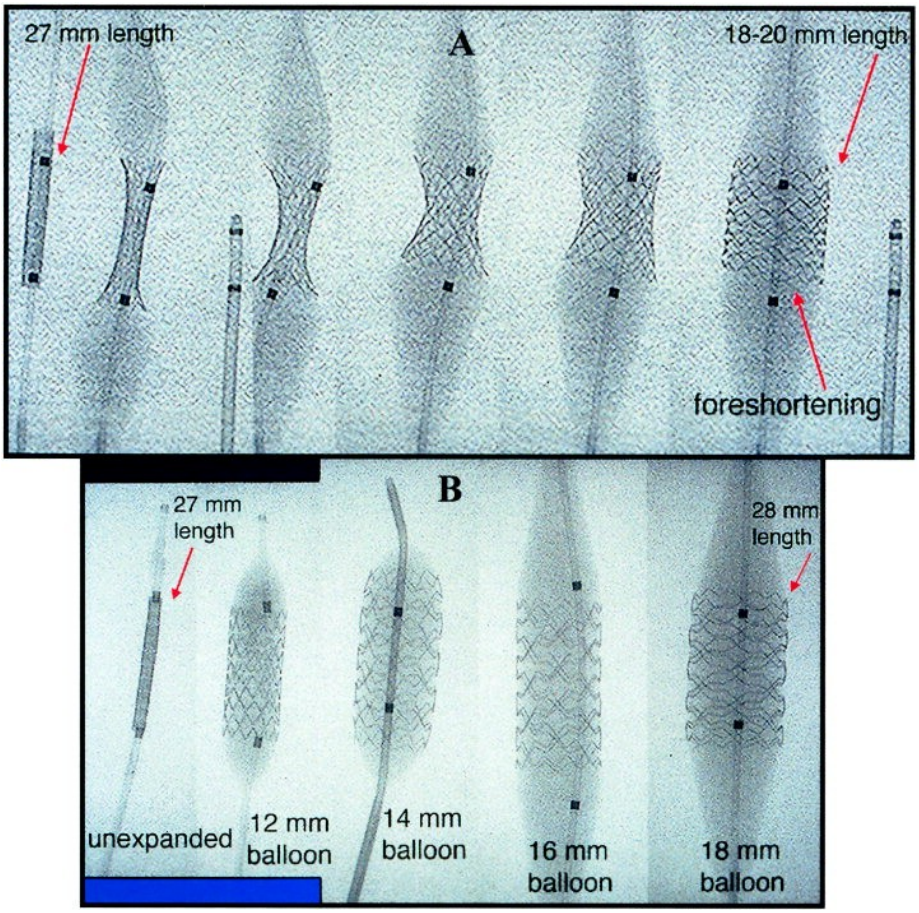

Figure 1.21: Expansion of DoubleStrut LD A) single balloon inflation results in 26-33% FS, whereas B) With serial balloon expansion, there is no FS. From [32]

- **Mega LD stent**: The Mega LD is from the same family as the Doublestrut LD. It has the same *open cell* design and the same rated diameter (12mm). However, the Mega LD offers greater radial strength than the Doublestrut LD as it is cut in a thicker stainless steel tube. Again, serial dilation is key to appropriate deployment without significant foreshortening [13]. Numerical data on foreshortening is not available at this time.

- **Genesis Extra Diameter (XD) stent**: is the larger version of the Genesis stent described earlier. The Genesis XD can be deployed up to 18 mm while still retaining comparable radial strength to the Palmaz 8 series and showing approximately equivalent foreshortening [70]; see table 1.3.

This stent has become the standard for treatment of most congenital vascular stenoses for which the adult diameter won't exceed 18mm. It is expected that it will replace the Palmaz 8 series of stents in most central vessels for congenital lesions [13, 32, 70].

- **Cheatham Platinum (C-P) stents**: As opposed to the stents described above, the CP-stent has been designed specifically to answer the needs of the pediatric population, namely to accommodate for somatic growth while offering minimal foreshortening (<20%). The CP stents are manufactured from 90% platinum, 10% iridium wires arranged in a zig pattern; rows of zigs are laser-welded to form a cylindrical meshwork. They are offered as bare stents or covered with an expandable sleeve of ePFTE both for native or recurrent aortic coarctation depending on the clinical conditions (Figure 1.22) [73]

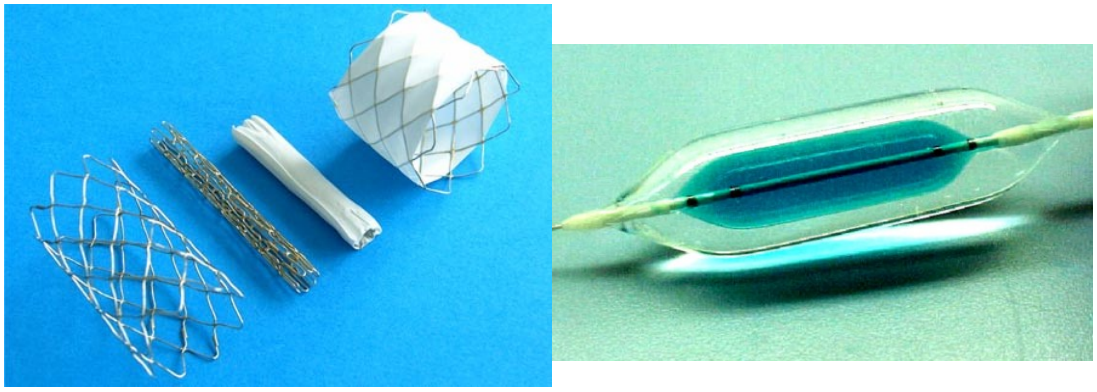

Figure 1.22: a) Bare and covered Numed CP stents; b) BIB catheter. From [73]

Six or eight zig stents are offered, depending on the adult target vessel diameter: maximum expanded diameters are 15 to 24mm with offered lengths varying from 16 to 50mm. Custom made 10-zig stents have a potential maximal diameter of 30mm with less than 20% foreshortening, requiring however larger introducer sheaths. Cheatham J. also developed a balloon catheter as well: The balloon-in-balloon catheter (BIB) allows for serial dilation to

large diameters, while using a single catheter: with the inner balloon, the stent is first uniformly expanded to half its diameter; the outer balloon is then inflated to the final diameter [24, 74]. Experimental studies demonstrated that the 6-zig CP stent offered lower radial strength than that of the Palmaz at large diameters whereas the 8-zig stent showed good radial strength. As for foreshortening, it varies from 8 to 28% depending on the number of zigs and expanded diameter (see Tables 1.3 and 1.4).

The wide range of available sizes and the small extent of foreshortening render the CP stent an interesting alternative for the pediatric interventionist. Moreover, because of its composition, the CP stent is very radio-opaque and MRI safe. On the other hand however, it is a rather stiff stent that is only available as a special order by prescription in Canada and the US; it has however CE (*Conformité Européene)* mark approval for use in Europe [73].

Table 1.3 below summarizes some key characteristics of the large stents described above as well as their advantages and disadvantages.

	Non expanded diameter	Rated diameter	Maximal diameter	Foreshortening		Available Lentghs	Sheath sizes	Advantages	Disadvantages
				%	At D				
Palmaz 8 series	3.4mm	8mm	18-20 mm	3%	8mm	12, 18, 30 mm	7-11 Fr	• Long-standing history of use in pediatric cardiology • Good radial strength	• Rigid; • Overdilation met with significant stent resistance during deployment; • Foreshortening at large diameters.
				25%	10mm				
				<33%	12mm				
				40-50%	18-20mm				
Doublestrut LD	3.8mm	9-12mm	18-20mm	None	12mm	16, 26, 36, 56, 76 mm	7-11Fr	• Rounded ends and edges; • Comparable radial strength to Palmaz, up to 12mm expansion; • Very flexible	• At expansion >15mm, it lacks the radial strength of Palmaz; • Tends to recoil immediately after implant or collapse under high wall stress in large diameter vessels. • Can distort with overexpansion due to an increase in cell size.
				6%	15mm				
				23-34%	18mm				
				None	18mm Serial dilation				

	Non expanded diameter	Rated diameter	Maximal diameter	Foreshortening		Available Lentghs	Sheath sizes	Advantages	Disadvantages
				%	At D				
Genesis XD	N/A	10-12mm	18mm	7%	10mm	19, 25, 29, 39, 59mm		• Good radial strength, comparable to Palmaz • Very flexible • Less foreshortening than Palmaz	• Rare reports of separation at the omega hinges
				16%	15mm				
				20-34%	18mm				
Mega LD	3.8mm	9-12mm	18mm	None	15-18mm (serial dilation)	16, 26, 36mm	9Fr	• Flexible • Rounded edges • No foreshortening with sequential dilation at 18mm with similar radial strength to Palmaz.	• Manipulation immediately after implantation can result in the tip of the catheter pushing cells out of shape. Re-maniulation or redilation reserved after stent has fixed into tissues.
				<25%	At largest diameters (single dilation)				

	Non expanded diameter	Rated diameter	Maximal diameter	Foreshortening		Available Lentghs	Sheath sizes	Advantages	Disadvantages
				%	At D				
CP six-zig	N/A	15-18mm	18mm	20-27%	18mm	16 to 45mm	10-12Fr	• Rounded edges; • Ni significant foreshortening at largest diameters; • Radio-opaque; • MRI-safe.	• A rather stiff stent compared to other available stents, but less stiff than Palmaz; • Lower radial strength at expanded diameters >14mm.

Table 1.3: Key characteristics of large stents

D) Extra-Large stents

Extra-large stents can be expanded to maximum diameters of 24-25 mm. They are used in treatment of very large central vessels: the aorta, large right ventricular baffles or homografts and Fontan baffles. This group includes: Palmaz XL series, Maxi LD and CP eight-zig stent.

- **Palmaz 10 series:** Palmaz 10 series of stents is manufactured of a slightly thicker and larger diameter tubing with larger and longer cells than in the Palmaz 8 series. Moreover, each row has 11 cells (as opposed to 7 in the smaller versions). Experimental tests reported excellent radial strength with 23% foreshortening at 25mm expansion [13, 32].
- **Maxi LD stent:** Maxi LD is a larger, thicker version of the previously described Mega LD. It can be expanded up to 26mm without significant foreshortening if dilated sequentially. However, when crimped on a large BIB balloon, the stent shows considerable resistance to the start of the expansion of the inner balloon and the latter must usually be inflated at pressures 3 to 4 atm larger than the rested burst pressure o the inner balloon [13].
- **CP eight-zig stent:** This stent which is also part of the large stents has been described in section C) above.

Figure 1.23 below shows expanded CP eight-zig stent and a Palmaz XL (or 10 series) stents both deployed to 24mm diameter.

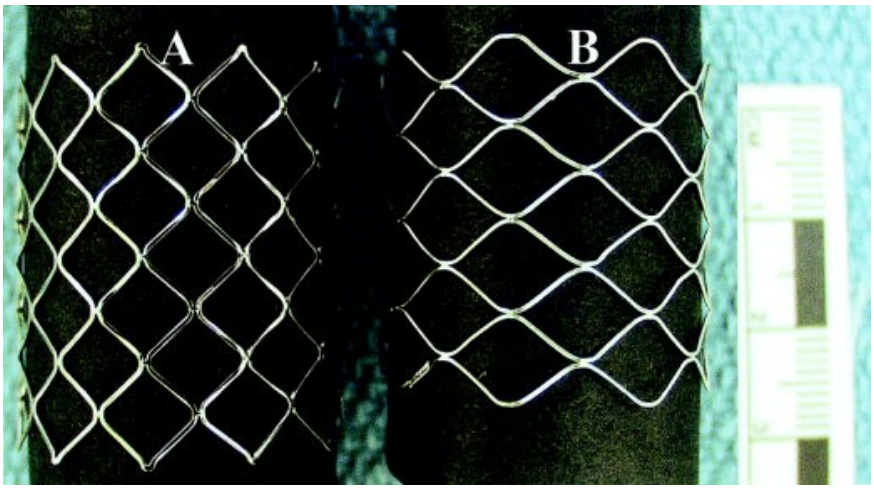

Figure 1.23: A) Palmaz XL and B) CP eight-zig stent expanded to 24mm. From [32]

Table 1.4 below summarizes some key characteristics of the extra-large stents described above as well as their advantages and disadvantages.

	Non expanded diameter	Rated diameter	Maximal diameter	Foreshortening		Available Lengths	Sheath sizes	Advantages	Disadvantages
				%	At D				
Palmaz 10 series	N/A	10mm	25mm	9-10%	18mm	30-50mm	11-13Fr	• Smoother edges than other Palmaz series; • Good radial strength;	• Stiff; • Large sheaths
				12-13%	20mm				
				23%	25mm				
Maxi LD	4.5mm	12mm	24-26mm	<25%	At largest diameters (serial dilation)	16, 26, 36mm		• Flexible • Rounded edges • No foreshortening with sequential dilation. • Wall strength comparable to Palmaz 8 series up to 24mm expanded diameters	• Significant resistance when deployed on BIB balloon: the inner balloon must be inflated with pressures 3 to 4 atm greater than the rated burst pressure of the inner balloon.

	Non expanded diameter	Rated diameter	Maximal diameter	Foreshortening		Available Lentghs	Sheath sizes	Advantages	Disadvantages
				%	At D				
CP eight-zig	N/A	24mm	24mm	8-15%	18mm	16 to 50mm	11-13Fr	• Good overall radial strength • Rounded edges; • No significant foreshortening at largest diameters; • Radio-opaque; • MRI-safe.	• Requires sheaths 2Fr larger than the implantation balloon; • Difficult to crimp stent to diameters smaller than 8 or 9Fr; • A rather stiff stent compared to other available stents, but less stiff than Palmaz.
				22-28%	24mm				

Table 1.4 : Key characteristics of extra-large stents

1.6.2. Novel stent developments for congenital heart disease

Stents presented in section 1.6.1 above are permanent stents: once implanted, they are endothelialized and integrated into the vessel wall with the only possibility of accommodation of somatic growth, when necessary, being surgical removal of the stent and patch correction of the arterial wall. Novel developments in stenting include stents which are biodegradable as a whole or with a combination of biodegradable sutures and permanent implant materials. These stents are described in greater detail below.

A) Growth stent: The growth stent (*QualiMed, Germany)* has been designed with the idea of a stent small enough to be implanted in infants and small children while it is still able to be dilated to the adult vessel diameter without creating a steel-lined obstruction. Therefore, the stent consists of two longitudinal, laser cut and electropolished stainless steel halves connected by bioresorbable sutures. The sutures are secured in tongue and groove elements to avoid longitudinal sliding and provide greater radial support (Figure 1.24) [75]. Stents can be made in lengths from 14 to 18 mm and sutures can be parallel or diagonal. The time period over which the circular shape of the stent is preserved depends on the type of bioresorbable suture used.

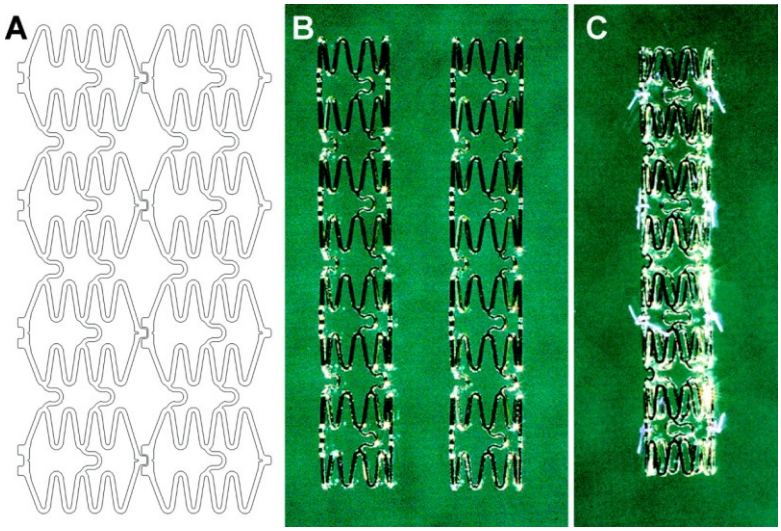

Figure 1.24: Growth stent A) 2-D drawing, B) Two halves C) Complete sutured stent. From [75]

In their animal study, Ewert et al. [75] used Vicryl 7/10 (Polygalactin) which loses half its strength during the first two weeks and is completely resorbed after 8 weeks. The stent has been dilated in the aorta, pulmonary arteries and inferior vena cava of 13 piglets, to diameters ranging from 3 to 8mm and introduced via 5Fr introducer sheaths. At 7mm, stent foreshortening was noted to be about 15%. Recatheterization has been performed after a mean period of 18 weeks. In 50% of the cases, a reduction of 10% in vessel diameter occurred which was relieved by

successful balloon redilation. Histopathology showed no excessive neointimal proliferation with foreign body reaction seen at the sites of the sutures. According to the authors, whether remaining radial forces after absorption of sutures can prevent restenosis of abnormal walls has to be evaluated.

In 2008, Ewert et al. published results in a clinical setting (aortic coarctation) for the growth stent [76]. In that study, the suture material used was Polydioxanon which loses half its strength after the first 5 weeks and is completely resorbed after 6 months. Thirteen (13) growth stents have been implanted in 12 patients through 5Fr sheaths. In a follow-up period of 24 months, five patients had one or two ballon dilations whereas six of them received a commercially available large stent.

The authors conclude that the adaptive growth of the stented area noted in the animal study has not been reproduced and therefore suggest the possibility of using the growth stent as a bridge therapy for infants until they reach a body weight of about 12kg, at which point they can receive a larger conventional stent that has the ability to be expanded to adult diameters.

It must be noted that the idea of a *split* or *open stent* has first been introduced by Ing et al. in 1996 [77, 78]. However, whereas the growth stent has two longitudinal splits and is manufactured as two separate halves, the stent introduced by Ing et al. was a modified stent with one longitudinal split, an *open-ring* stent. Moreover, it did not use bioresorbable sutures.

B) Breakable stent (*Dr. Osypka, GmbH, Germany)*: This stent is similar to the previously described *open-ring* stent by Ing et al. The breakable stent however, is not hand-cut but rather manufactured including the single longitudinal cut and eyelets for bioresorbable sutures (Prolene 6-0) attachment (Figure 1.25). The stent has a standard coronary stent design and is made out of stainless steel 316L, and is covered with gold to improve its visibility under fluoroscopy. It can be introduced through 4-5Fr sheaths [79].

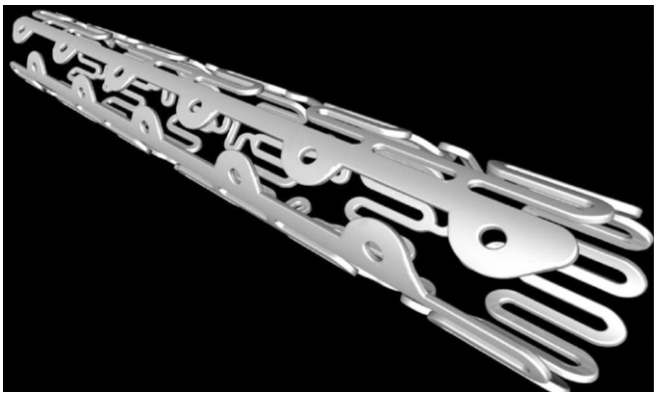

Figure 1.25: 3-D Computer Aided Drawing (CAD) of the breakable stent

Sigler et al. published an animal study which showed the ability of the stent to be redilated (or *broken open*) with balloon catheters up to 125% the vessel diameter and adapt to vessel growth (redilations were performed between 18 and 165 days after implantation, in piglets).

Histology revealed complete cellular coverage of the stent with mild intimal hyperplasia and mild inflammatory reaction of surrouding tissue. No foreign body reactions were seen. Authors conclude that the breakable stent can help avoid surgery to remove stent in infants and neonates due to vessel growth or at least postpone it.

C) Biodegradable stent

C.1) Polymer stents

A degradable stent that would temporarily withstand radial forces at the narrowing site as the vessel heals and then disappear would be an ideal solution to relieve stenoses in growing children.

The first quests for biodegradable stents studied the use of various polymers in porcine coronary artery models. However, results have been disappointing as polymers proved to be associated with significant inflammatory response, neointimal proliferation or thrombus formation and vessel occlusion [80]. Tamai et al., on the other hand, were the first to report successful implantation of a poly-L-lactic acid (PLLA) biodegradable stent in human coronary arteries (Figure 1.26). At 6 months and 1 year follow-up, acceptable neointimal formation was noted, comparable to that of stainless steel stents with restenosis rates of 21 and 19% at 6 and 12 months respectively [81-85]. Recently, results of 4 years follow up showed satisfying long term results with event free survival of 82% [86]. The stent is made of a PLLA monofilament arranged in a zigzag helical coil design, with two gold markers. The available dimensions are expanded diameters ranging from 3 to 4.5mm, and 12mm in length [87]. It is a self expanding stent but a custom-made balloon catheter can be used as well. However, it is unable to fully expand with balloon dilatation and application of heat is necessary, rendering it possibly harmful to the vessel wall. Moreover, the stent is made out of a thicker material (0.17 and 0.24mm) than conventional stents because of the lower radial force of the polymer, and is still associated with acute recoil of 22% [88].

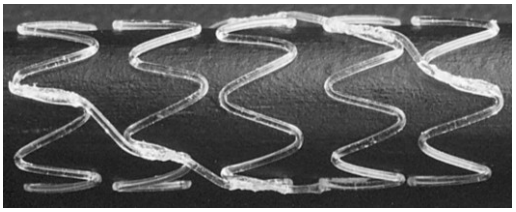

Figure 1.26: Igaki-Tamai PLLA stent. From [87]

C.2) Absorbable Metal Stents (AMS)

A biocorrodible metal stent offers the potential to be resorbed while overcoming the shortcomings of polymeric stents as to their mechanical characteristics.

Heublein et al. first described the use of a magnesium stent in an animal model in 2003 [89]. Magnesium is one of the most important micronutrients of the human body therefore side effects of its degradation products are expected to be unlikely [88]. Moreover, it has been shown in animal studies that Mg degrades into calcium phosphate crystals [90]. This first simple design used AE21 alloy for its degradation kinetics (six months expected half life) however, in vivo, the stent degraded four times faster than expected with loss of mechanical integrity 35 days after implantation. The complete breakdown of the stent was estimated to be in the order of three months in vivo. As for neointimal proliferation, there was a significant increase up until the 35th day, after the increment was insignificant. This is explained by the inflammatory reaction to the degradation products and the extent to vessel wall injury, which influences the extent of neointimal proliferation. The stent had a variable thickness (150-200 microns) which resulted in uneven expansion and greater vessel wall injury around some of the struts. This first magnesium stent offers the possibility of absorbable metal stents to present a promising new technology that however needs further improvements as to the design technology as well as the degradation time to maintain necessary mechanical stability for healing to occur.

A use of another magnesium alloy (WE43) with different degradation kinetics has been successfully implanted in animals, and later implanted into the lower leg arteries of adult patients [88, 91]. The Lekton Magic stent *(Biotronik, Switzerland)* has a maximal undeployed diameter of 1.2mm and can be deployed to 3mm through a 6Fr catheter, with two lengths available 10 and 15mm (Figure 1.27) [88].

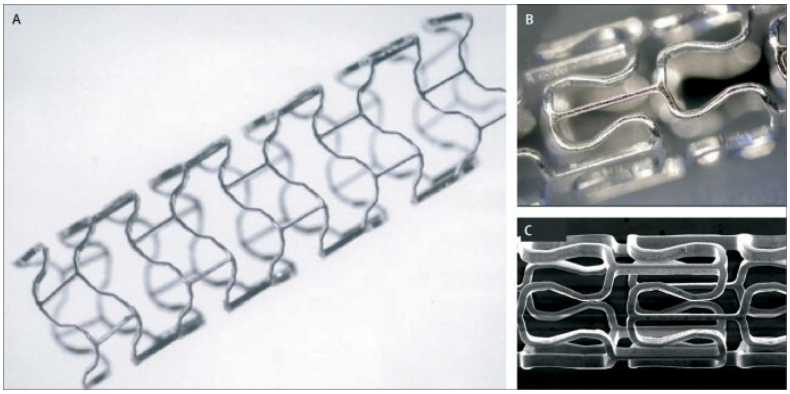

Figure 1.27:(A) after expansion, (B) before expansion, and (C) in an electron microscopy magnification. From [92]

A multicentre non-randomized trial is ongoing for implantation in human coronary arteries [92]. Preliminary results show the ability of the stent to be used as temporary scaffolding to decrease diameter stenosis from 61.5% to 12.6%. However, following stent degradation at 4 months, in 47.5% of the 63 patients enrolled, diameter stenosis was noted to be 48.4% mainly due to neoinitmal growth. Major cardiac events defined as repeat percutaneous intervention, bypass surgery and restenosis occurred in 23.8% of the patients at 4 months and in 26.7% at one year follow-up. There were no deaths, myocardial infarctions or thrombosis reported up to one year after implantation.

There have been two single case reports of the use of the Lekton Magic stent in children: one in a left pulmonary artery (LPA) of a preterm [93, 94] and one in recoarctation of the aorta in a newborn [95].

In the first case of a severely preterm baby, the stenosis was inadvertently created when the LPA was ligated in an attempt to ligate the arterial duct. After surgical removal of the ligature, angiography still revealed a complete occlusion of the LPA. The implantation of a 3mm (expanded diameter) magnesium stent was done intra-operatively as the LPA was sharply bent and percutaneous stenting was not possible. The major concern with the use of a magnesium stent in this case was the possibility of attaining high toxic magnesium levels during the degradation process because of the low total blood volume. The maximum level was noted the second day post-implantation and declined thereafter, suggesting endothelial covering of the stent and its isolation from circulating blood. No recoil was noted immediately after implantation and adequate left lung perfusion was not noticed immediately after the procedure but after one week. At 33 days follow-up, adequate lung perfusion remained. At 5 month follow-up, after complete stent degradation, left lung was still perfused with a minor difference in size between the LPA and

RPA (0.7/1 ratio). The reduction in luminal area appeared to be the result of a combination of neointimal growth and stent degradation. Shortly after, the patient suffering from severe pneumonia died from multiple organ failure. With the parents' consent, macropathological and histological data could be gathered. The inner lumen diameter of the LPA was measured to be 3.7mm suggesting the vessel was growing (RPA was 7mm). Stent disintegration was complete and bulks of calcium-phosphate material replaced the metal struts as expected. Moreover, cellular infiltration of the CaP islands suggested cellular substitution of the stent remains by cells. In addition to the former, mild intimal proliferation may indicate that neointimal proliferation as stimulated by the foreign materials had declined after 5 months suggesting that intimal hyperplasia gradually declines as stent degrades and byproducts are substituted by cells. Finally, no foreign body reaction was seen at the site of calcium phosphate materials [89].

In the second case, a 3 week old newborn, suffering from critical aortic coarctation received corrective surgery. However, recoarctation became evident intraoperatively.
A 15mm Lekton stent was successfully implanted and deployed to 4mm. After 3 weeks, because of the stent degradation process, luminal diameter decreased to 2-2.8mm, a second magnesium stent was then implanted. At the age of three months, VSD closure had to be performed because of excess right to left ventricular shunting. Surgical patch augmentation of the stented aortic segment was performed as well since there was a systolic pressure gradient of 20 mmHg over the stented segment. The previously stented vessel was flexible as there were only some residual metal struts [95]. While recognizing the limitations of a single case report, authors believe that the absorbable metal stent may be a promising therapy for recoarctation and native coarctation in newborns.

Finally, the review of biodegradable stents presented above is not comprehensive as various other design are under study for treatment of coronary artery disease, including bioabsorbable drug eluting polymer stents such the REVA and Paclitaxel polylactide stents to name a few[96, 97].

Although a lot of progress has been made in the area of bioabsorbable stents over the last 3 years[86], further developments are required before these stents become candidates to replace conventional bare metal stents, especially in congenital heart disease applications.

1.7. Effect of stent design parameters and deployment techniques on tissue response

Various parameters in stent design and deployment techniques greatly affect the tissue response in the stented vessel segment.

As explained earlier, intimal hyperplasia that is a thickening of the intima following trauma, is a normal healing process. Angioplasty is in fact a traumatic event during which tearing of the arterial layers appears to be a dilating factor in a stenosis [8, 60]. Nevertheless, the mechanisms of in-stent restenosis are poorly understood as conflicting explanations exist. Effectively, it has been shown that tearing of the intima and the media and their healing thereafter seem to contribute to relief the stenosis [16, 98], with the most effective relief occurring with a deep medial tear. On the other hand, deployment at higher pressures and stents with sharp edges for example result in greater vessel wall injury which may in turn lead to greater intimal proliferation [23, 99]. Therefore, deployment strategies that would reduce medial damage and avoid stent oversizing may lower the frequency of in-stent restenosis [100].

Stent design parameters affect the extent of neointimal thickening as well. It has been shown that the number of stent struts affect tissue response independently of arterial injury. In fact, Garasic et al. compared the effect of the number of struts while imposing similar vessel injury scores [101]. Increasing the number of struts from 8 to 12 per cross section resulted in a two-fold reduction of neointimal thicknening after 28 days.

Moreover, stents with greater hoop strength proved to have significantly less recoil and neointimal proliferation than stents with lower radial strength [102]. On the other hand, thinner stent struts (50 microns vs. 140 microns) are associated with less restenosis rates [103, 104]. Other reports however state that strut thickness did not seem to affect late intimal thickening (125 vs 200 microns) [101].

Finally, stent profile also plays a role in wall cellular response. In fact, higher profile stents are associated with higher hyperplasia. This is explained by the fact that under scanning electron microscopy, it can be seen that the formed neointimal layer attempts to level the *valleys* between the *hills* caused by the stent struts rising over the luminal surface (Figure 1.28) [102].

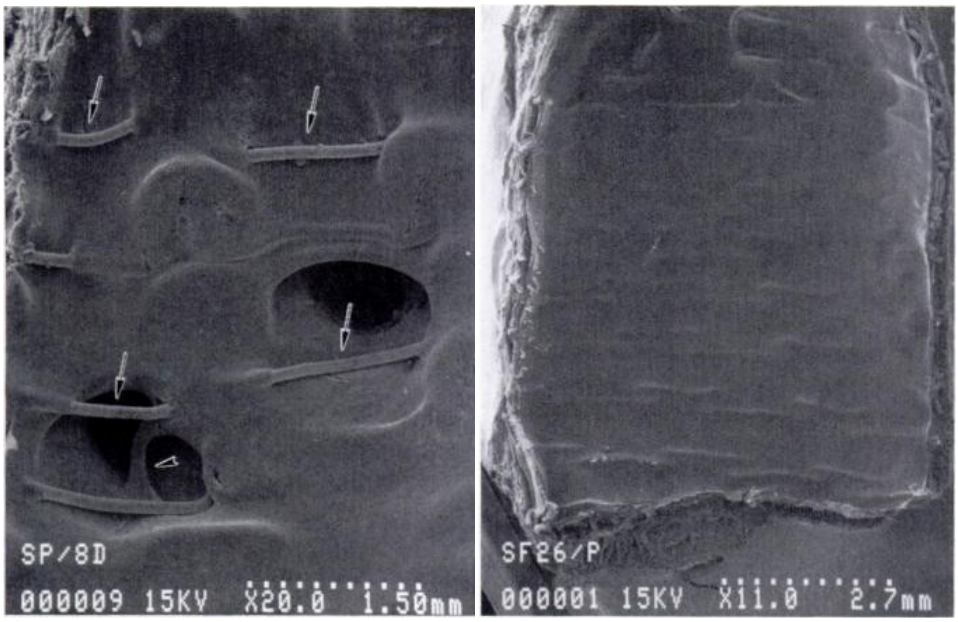

Figure 1.28 : SEM of the endothelial surface from the aorta in canine model a) at 8 weeks after placement of high profile stent; b) at 26 weeks after implantation. From [105]

Please note that data in this section applies mainly to coronary artery stenting as the latter is much more documented in the literature than pediatric stenting. Nevertheless, histological findings in experimental aortic coarctation in puppies showed the same results as those reported in coronary arteries[106]. In fact, intimal hyperplasia in adults is caused by fracture of the internal elastic lamina and migration of the smooth muscle cells and fibroblasts from the media to the intima and their proliferation; the same changes were found in the experimental study in puppies.

Moreover, it has been shown that medial tearing, flapping and arterial wall dissection during balloon angioplasty of the aorta was associated with a dilation ratio of more than 50% whereas patients with a ratio less than 50% has superficial tearing of the arterial wall or stretching [107].

1.8. Thesis objectives

In the light of the problematic and challenges described above, as well as the available resources to the pediatric interventionist, we will now state the rationale of the present project.

The thesis goals are to optimize, from a structural point of view, a novel stent design for relieving stenosis in pulmonary arteries in children.

The main goal is to design a novel stent that is suitable for older children as well as young infants without the risk of creating an iatrogenic stenosis and requiring surgery. The designed stent should address other limitations of adult stents such as foreshortening, while offering good radial support until complete endothelialization of the stent (about 6 months). Moreover, the stent should be readily deployable on existing delivery balloon catheters.

Emphasis will be mainly put on the structural design aspects, while keeping in mind that the project is multidisciplinary and various factors come into play.

In the following chapters, the mathematical background and the equations governing the phenomenon of stent deployment will be presented. The engineering design process will be presented including a detailed description of the design requirements, the optimization steps and tools used to achieve the final design.

2. Structural mechanical models for investigating a stent behaviour

Prior to introducing the design requirements and design optimization steps, it is worthy to present a brief mathematical background and the governing equations that apply to our problem.
First of all, the deployment of a stent on a balloon is a nonlinear structural mechanics problem which entails two types of nonlinearities: material nonlinearity and geometric nonlinearity.

2.1. Material nonlinearity

Ductile metals such as stainless steel obey Hooke's law only in a certain range of small strain. When load is further applied, a certain level of stress is reached and there is a gradual transition from linear elastic to non-linear plastic behavior. The relationship between stress and strain is non linear, and path-dependent (The stress not only depends on the strain but on the strain history as well) [108, 109]. Once the load is removed, irreversible permanent straining occurred.

The theory of plasticity is based on three fundamental concepts: the yield criterion which defines the limit at which the material becomes plastic, the flow rule which relates the stresses and strains once the material is in the plastic range and the hardening rule which studies the change in shape and size, or translation of the yield surface.

2.1.1. Yield criterion

A key assumption in the theory of plasticity is the existence of a continuous scalar yield function which basically defines the limit at which the material becomes plastic [110, 111]

$$f(\sigma_{ij}, \alpha_{ij}) = 0 \tag{1}$$

where σ_{ij} are the stresses and α_{ij} are internal parameters of the material

$f < 0$, represents the elastic range
$f = 0$, represents yielding
$f > 0$, is physically impossible

Geometrically, the state of stress at any point in the material can be described in a nine dimensional stress space with axes σ_{ij} (i,j=1,2,3). Around the origin of the stress space, there exists a domain of elastic range, the boundary of which defines a surface known as the *initial yield surface* [110, 112].

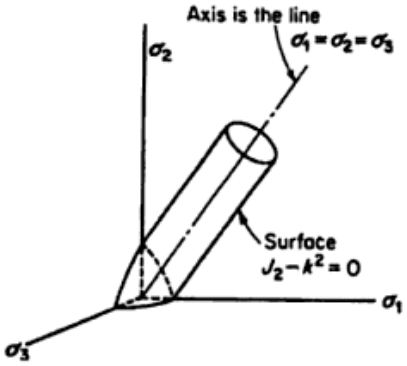

Figure 2.1: A yield surface in the principal stress plane. From [110]

As a simple representation, figure 2.2 below shows a yield surface in two dimensions.

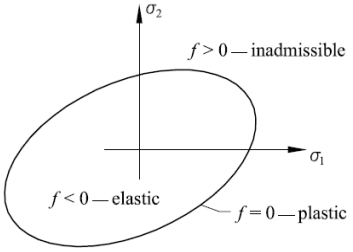

Figure 2.2: 2-D yield surface. From [111]

For an isotropic material, the material properties are the same in all directions, the yield function can therefore be expressed in terms of the principal stresses or the invariants of the stress tensor: $f = f(\sigma_1, \sigma_{2,} \sigma_3)$ or $f = f(I_1, I_{2,} I_3)$. Moreover, experiments conducted with metals showed that hydrostatic compression or tension does not cause significant plastic deformation. Therefore, the yield function can also be expressed in terms of the invariants J_2 and J_3 ($J_1 = 0$) of the stress deviation tensor $f = f(J_2, J_3, \alpha_{ij})$ [113].

The stress deviation tensor $\sigma_{ij}^{'}$ is defined as [110]:

$$\sigma_{ij}^{'} = \sigma_{ij} - \sigma_m \delta_{ij} \tag{2}$$

Where δ_{ij} is the Kronecker delta

$\sigma_m = 1/3(\sigma_1 + \sigma_2 + \sigma_3)$ is the mean stress

The stress deviation tensor invariants J_2 and J_3 are given by [114]:

- $J_2 = \frac{1}{2}(\sigma_{ij}^{'}\sigma_{ij}^{'})$

  $= I_2 + \frac{1}{3} I_1^2$

$$J_2 = \frac{1}{6}\left[(\sigma_1 - \sigma_2)^2 + (\sigma_2 - \sigma_3)^2 + (\sigma_3 - \sigma_1)^2\right]$$

- $J_3 = (\sigma'_1\, \sigma'_2\, \sigma'_3)$

$$= \frac{1}{3}(\sigma_1^{'3} + \sigma_2^{'3} + \sigma_3^{'3})$$

$$J_3 = \frac{1}{27}(2\sigma_1 - \sigma_2 - \sigma_3)(2\sigma_2 - \sigma_3 - \sigma_1)(2\sigma_3 - \sigma_1 - \sigma_2)$$

von Mises criterion

First, the von Mises yield condition is defined by the yield function:

$$f(J_2) = J_2 - k^2 = 0 \tag{3}$$

Where J_2 is as defined above and k is a constant

It can be shown that $k = \frac{\sigma_y}{\sqrt{3}}$, where σ_y is the uniaxial yield stress [112].

Equation 2 can therefore be written as:

$$J_2 - \left(\frac{\sigma_y}{\sqrt{3}}\right)^2 = 0$$

$$\sqrt{3}J_2 - \sigma_y = 0 \tag{4}$$

The yield function can also be written in terms of the von Mises stress:

$$\boxed{f(\sigma_{ij}) = \sigma_{VM} - \sigma_y = 0} \tag{5}$$

From (3) and (4), it follows that:

$$\sigma_{VM} = \sqrt{3J_2}$$

$$\boxed{\sigma_{VM} = \sqrt{\frac{1}{2}\left[(\sigma_1 - \sigma_2)^2 + (\sigma_2 - \sigma_3)^2 + (\sigma_3 - \sigma_1)^2\right]}} \tag{6}$$

Geometric representation

From (30, (4) and (6), the von Mises criterion equation can also be written as:

$$(\sigma_1 - \sigma_2)^2 + (\sigma_2 - \sigma_3)^2 + (\sigma_1 - \sigma_3)^2 = 6k^2 = 2\sigma_y^{\,2} \tag{7}$$

In a 3-D principal stress space, the yield surface is represented by a right cylinder whose axis is equally inclined to the three axes of reference. The deviatoric plane $\sigma_1 + \sigma_2 + \sigma_3 = 0$ intersects the yield surface in a closed curve, the yield locus. The yield locus is a circle with radius $\sqrt{2/3}\sigma_Y$

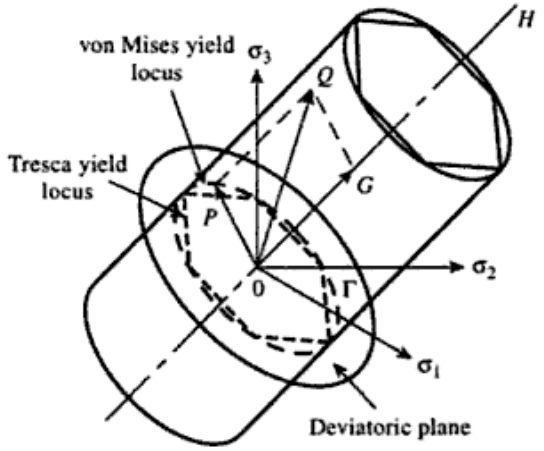

Figure 2.3: Geometrical representation of yield criteria in the principal stress space. From [112]

Prior to introducing the flow rule, it is worth to present the consistency condition which is a key condition in the plasticity theory. This condition prevents the stresses from exceeding the yield limit in perfect plasticity. In fact, a stress point on the yield surface may remain in one fixed position or slide along it during plastic loading. Mathematically [110, 111]:

$$df = \frac{\partial f}{\partial \sigma_{ij}} d\sigma_{ij} = 0 \tag{8}$$

Equation (8) is known as the consistency condition for ideal plasticity.

2.1.2. Flow rule

Because there is no unique relationship between stresses and total strains in the plastic range, it is convenient to consider only plastic strain increments $d\varepsilon^P$. The total strain increment is assumed to be the sum of the plastic and elastic strain increments [111]:

$$d\varepsilon = d\varepsilon^e + d\varepsilon^p \tag{9}$$

von Mises suggested that there exists a plastic potential function $h(\sigma_{ij})$ so that the plastic strain increment can be derived [110]:

$$d\varepsilon_{ij}^p = d\lambda \frac{\partial h}{\partial \sigma_{ij}} \tag{10}$$

$d\lambda$ is a scalar called the plastic multiplier which determines the amount of plastic straining, or mathematically, the magnitude of the increment, whereas *h* determines the direction of plastic straining [109].

Equation (10) is known as the flow rule and it is termed associative flow rule when the plastic potential function *h* is the yield function *f*, that is *h=f*; and non-associative when $h \neq f$. However, experimental observations have shown that the associative flow rule characterizes quite well the plastic deformation of metals [110] therefore:

$$d\varepsilon_{ij}^{p} = d\lambda \frac{\partial f}{\partial \sigma_{ij}} \tag{11}$$

Using the associated flow rule in (11), the plastic strain increments can be determined for the von Mises yield criterion

$$d\varepsilon^{P} = \begin{bmatrix} d\varepsilon_{x}^{p} \\ d\varepsilon_{y}^{p} \\ d\varepsilon_{z}^{p} \\ d\gamma_{xy}^{p} \\ d\gamma_{yz}^{p} \\ d\gamma_{zx}^{p} \end{bmatrix} = d\lambda \frac{1}{2\sigma_{VM}} \begin{bmatrix} 2\sigma_{x} - \sigma_{y} - \sigma_{z} \\ 2\sigma_{y} - \sigma_{z} - \sigma_{x} \\ 2\sigma_{z} - \sigma_{x} - \sigma_{y} \\ 6\tau_{xy} \\ 6\tau_{yz} \\ 6\tau_{zx} \end{bmatrix} \tag{12}$$

The usefulness of the plastic strain increment will be shown later in this section.

2.1.3. Hardening rule

Following the yield function and the flow rule, the third aspect to be considered in the plasticity theory is the hardening rule that is how the initial yield surface changes as yielding progresses [110]. There exist two hardening rules (Figure 2.4):

1) Isotropic hardening: assumes that material remains isotropic during plastic loading and the subsequent yield surface is simply an expansion of the initial yield surface, with both surfaces having the same center.

2) Kinematic hardening: predicts the development of anisotropy; the yield surface remains constant in size and shape, but it translates [112].

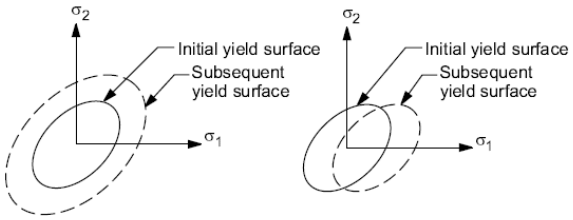

Figure 2.4: Types of hardening rules a) Isotropic work hardening b) Kinematic hardening. [109]

2.1.4. Plastic work

The hardening rule presented above states that the yield function changes with hardening. Rewriting the yield function to incorporate these changes[109]:

$$f(\{\sigma\}^T, \kappa, \{\alpha\}) = 0 \tag{12}$$

κ is the plastic work

$\{\alpha\}$ is the translation of the yield surface

κ and $\{\alpha\}$ are called internal or state variables

The plastic work is the sum of the plastic works done over the history of loading and is defined as:

$$\kappa = \int \{\sigma\}^T [M] \{d\varepsilon^p\} \tag{13}$$

$$d\kappa = \{\sigma\}^T [M] \{d\varepsilon^p\} \tag{14}$$

$$[M] = \begin{bmatrix} 1 & 0 & 0 & 0 & 0 & 0 \\ 0 & 1 & 0 & 0 & 0 & 0 \\ 0 & 0 & 1 & 0 & 0 & 0 \\ 0 & 0 & 0 & 2 & 0 & 0 \\ 0 & 0 & 0 & 0 & 2 & 0 \\ 0 & 0 & 0 & 0 & 0 & 2 \end{bmatrix}$$

The translation of the yield surface depends on the history of loading as well and is written as

$$\{\alpha\} = \int C\{d\varepsilon^p\} \tag{15}$$

$$d\alpha = C\{d\varepsilon^{pl}\} \tag{16}$$

C is a material parameter.

Equation (12) can be differentiated so that the consistency condition is:

$$df = \left\{\frac{\partial f}{\partial \sigma}\right\}^T [M]\{d\sigma\} + \frac{\partial f}{\partial \kappa} d\kappa + \left\{\frac{\partial f}{\partial \alpha}\right\}^T [M]\{d\alpha\} = 0 \tag{17}$$

Substituting (14) and (16) into (17) yields:

$$df = \left\{\frac{\partial f}{\partial \sigma}\right\}^T [M]\{d\sigma\} + \frac{\partial f}{\partial \kappa}\{\sigma\}^T [M]\{d\varepsilon^p\} + C\left\{\frac{\partial f}{\partial \alpha}\right\}^T [M]\{d\varepsilon^{pl}\} = 0 \quad (18)$$

2.1.5. Incremental $\sigma - \varepsilon$ relations in plastic flow

In elasto-plastic analyses, a load increment is usually applied. This load increment produces a displacement increment and thus a total strain increment. The stress increment corresponding to that total strain increment can then be determined using a constitute relation [111].

First, Hooke's law gives the relation between stresses and elastic strains:

$$d\sigma_{ij} = D_{ijkl}.d\varepsilon^e_{kl} \quad (19)$$

From (9), elastic strain increment $d\varepsilon^e_{ij} = d\varepsilon_{ij} - d\varepsilon^p_{ij}$:

$$d\sigma_{ij} = D_{ijkl}\left(d\varepsilon_{kl} - d\varepsilon^p_{kl}\right) \quad (20)$$

Substituting (11) into (20), we get:

$$d\sigma_{ij} = D_{ijkl}\left(d\varepsilon_{kl} - d\lambda\frac{\partial f}{\partial \sigma_{kl}}\right) \quad (21)$$

The plastic increment can be easily derived [113]:

$$d\lambda = \frac{D_{ijkl}\dfrac{\partial f}{\partial \sigma_{ij}}d\varepsilon_{kl}}{D_{pqrs}\dfrac{\partial f}{\partial \sigma_{pq}}\dfrac{\partial f}{\partial \sigma_{rs}}} \quad (22)$$

Note that there is a change in subscripts to avoid superfluous summations.

(22) into (21) and factoring $d\varepsilon_{kl}$ out yields:

$$d\sigma_{ij} = \left[D_{ijkl} - \frac{D_{ijrs}\dfrac{\partial f}{\partial \sigma_{rs}}D_{pqkl}\dfrac{\partial f}{\partial \sigma_{pq}}}{D_{pqrs}\dfrac{\partial f}{\partial \sigma_{pq}}\dfrac{\partial f}{\partial \sigma_{rs}}}\right]d\varepsilon_{kl} \quad (23)$$

Or

$$d\sigma_{ij} = D^{ep}_{ijkl}d\varepsilon_{kl} \quad (24)$$

D^{ep}_{ijkl} is the elasto-plastic constitutive matrix [110, 113].

Equation (24) is the general stress-strain increment relationship.

2.1.6. Finite element implementation

1- The stresses are computed based on a trial strain which is the total strain minus the plastic strain at the previous time step: $$\{\varepsilon_n^{tr}\} = \{\varepsilon_n\} - \{\varepsilon_{n-1}^{p}\} \quad (25)$$

The trial stresses are then computed using equation (17): $\left(\{\sigma^{tr}\} = [D^{ep}]\{\varepsilon^{tr}\}\right)$

2- The von Mises stress is evaluated; if it is less than the yield stress σ_y, the material is elastic and no plastic strain increment is calculated.

If it is greater than the yield stress σ_y, the plastic multiplier λ is approximated by a local Newton-Raphson iteration.

3- $\{\Delta\varepsilon^p\}$ is computed using (11).

4- The plastic strain is updated $\{\varepsilon_n^p\} = \{\varepsilon_{n-1}^p\} + \{\Delta\varepsilon^p\}$ and the elastic strain calculated:
$$\{\varepsilon^e\} = \{\varepsilon^{tr}\} - \{\Delta\varepsilon^p\}$$

5- The increments in the plastic work and the yield surface translation are computed via equations (14) and (16) and are updated ($\kappa_n = \kappa_{n-1} + \Delta\kappa$ and $\{\alpha_n\} = \{\alpha_{n-1}\} + \{\Delta\alpha\}$).

2.2. Geometric nonlinearity

Geometric nonlinearities arise in a structure when deformations are large enough to cause a change in geometry; the strains are no longer infinitesimal [115]. The stiffness of the material *K* is no longer constant, as it is a function of the displacements *u*. As a consequence, stiffness changes because the shape changes.

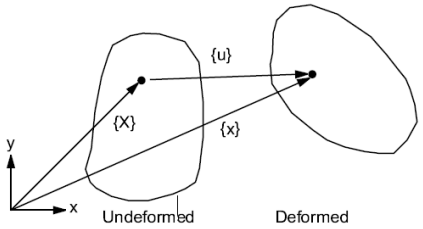

Figure 2.5: Position vectors and displacement of a deforming body. From [109]

The theory of large strains implies the use of a general mathematical relationship between motion and deformation. As shown in figure 30, let $\{x\}$ and $\{X\}$ be, respectively, the initial (undeformed) and final (deformed) position vectors of a point on the deforming body. Let $\{u\}$ be the displacement vector.

$$\{x\} = \{X\} + \{u\} \quad (26)$$

Differentiating with respect to X:

$$\frac{\partial\{x\}}{\partial\{X\}} = [I] + \frac{\partial\{u\}}{\partial\{X\}}, \qquad [I] \text{ the identity matrix} \quad (27)$$

The deformation gradient $[F]$ is defined as $[F] = \frac{\partial\{x\}}{\partial\{X\}}$.

Therefore,

$$[F] = [I] + \frac{\partial\{u\}}{\partial\{X\}} \quad (28)$$

The deformation gradient can be decomposed into a rotation and a shape change using the polar decomposition theorem [115]. The polar decomposition theorem is indeed useful for large strain and large rotation applications. The theorem states that the deformation gradient in (28) can be decomposed into a set of stretches followed by a rigid rotation.

$$[F] = [R][U] \quad (29)$$

In equation (29), $[R]$ is the rotation matrix ($[R]^T[R]=[I]$) and $[U]$ is the right stretch matrix. Note that the rotation can be followed by the stretch, therefore $[F] = [R][U] = [U_L][R]$ where $[U_L]$ is called the left stretch matrix. However, equation (29) is usually used.

At this point, various strain measures exist and are used in the large deformation theory, such as Green-Lagrangian strain or Eulerian (Almansi) strain. However, ANSYS (the FEM program used in this project) uses the Hencky or logarithmic strain which is defined as [113]:

$$[\varepsilon] = \ln[U] \quad (30)$$

As was the case for the plastic analysis, the strains are solved for through incremental approximation.

$$[\varepsilon] \approx \sum [\Delta\varepsilon_n]$$

with

$$[\Delta\varepsilon_n] = \ln[\Delta U_n] \quad (31)$$

2.2.1. Finite element implementation

The method used by ANSYS to evaluate equation (31) for 2-D and 3-D solid and shell elements has been proposed by Hughes et al [116].

The rotation-neutralized strain increment $[\Delta\varepsilon_n]^{RN}$ (or simply $[\Delta\varepsilon_n]$) is introduced:

$$[\Delta\varepsilon_n]^{RN} = [R_{1/2}]^T [\Delta\tilde{\varepsilon}_n][R_{1/2}] \quad (32)$$

- The strain increment $[\Delta\tilde{\varepsilon}_n]$ is computed from the midpoint configuration:

$$[\Delta\tilde{\varepsilon}_n] = [B_{1/2}]\{\Delta u_n\} \quad (33)$$

Where $\{\Delta u_n\}$ is the displacement increment over the time step.

$\lfloor B_{1/2} \rfloor$ is the strain-displacement matrix evaluated at midpoint geometry $\{X_{1/2}\} = \dfrac{\{X_n\} + \{X_{n-1}\}}{2}$

- $\lfloor R_{1/2} \rfloor$ in (32) is the rotation matrix evaluated at the midpoint configuration $[F_{1/2}] = [R_{1/2}][U_{1/2}]$

From equation (28), $$[F_{1/2}] = [I] + \frac{\partial \{u_{1/2}\}}{\partial \{X\}}$$

And the midpoint displacement is $\{u_{1/2}\} = \dfrac{\{u_n\} + \{u_{n-1}\}}{2}$,

$\{u_n\}$ is the current displacement,

$\{u_{n-1}\}$ is the displacement at the previous time step.

Finally, the computed strain increment $\left[\Delta\varepsilon_n\right]^{RN}$, or in vector form $\{\Delta\varepsilon_n\}$, can be added to the previous strain $\{\varepsilon_{n-1}\}$ to obtain the current total Hencky strain: $\{\varepsilon_n\} = \{\varepsilon_{n-1}\} + \{\Delta\varepsilon_n\}$.

This strain can then be used in the stress updating procedures in equation (25) in the previous section.

3. Design Optimization

One of the first steps in a design project is to clearly define the problem. This has been extensively covered in the first chapter (Section 1.6). Briefly, the problematic at hand is the use of unsuitable endoprostheses to treat PAS in infants. In fact, stents designed for the adult vascular system fail to effectively address the problem of congenital PAS. Moreover a new set of limitations arise due to the use of these stents (foreshortening, iatrogenic stenosis, etc).

In order to have a stent that will address the issues mentioned earlier, clear design requirements are to be devised. These are presented below.

3.1. Design requirements

Following the problem definition, one can introduce the design requirements for an ideal pediatric stent to treat pulmonary artery stenosis. Defining these requirements is a key step in the design process in order to factor in the human factors to be considered.

- First of all, as every prosthesis to be implanted inside the human body, the stent is to be biocompatible;
- The stent should be designed such that it accommodates for the child's growth, obviating the need for any subsequent surgery for stent removal. From childhood to adulthood, the lumen diameter of the pulmonary artery grows to approximately 18 mm. Therefore, the stent should be expandable over a wide range of diameters reaching adult sizes.
- The stent should be manufactured in a variety of diameters to answer the needs of children of different sizes.
- The stent should be flexible enough to pass through the tortuous vessels while maintaining sufficient structural integrity.
- The stent should allow its insertion through small sheaths;
- The stent should be deployable with pressures of 5 to 20 atm (Pressures used in the clinical setting) ;
- The stent should provide a good radial support during the healing period (about 6 months) and withstand wall forces;
- The stent should have minimal (<20%) or no foreshortening following expansion. It should effectively cover the stenosed area longitudinally;

- The stent should have minimal recoil following deployment;
- The stent should have no sharp ends or tips to minimize vessel trauma and risk of balloon burst.

3.2. Anterior designs

In our group, the original design idea for a pediatric stent that accommodates for child's growth was sketched by Dr. Galaz, R. The design was bio-inspired from a snake skeleton. In fact, simply stated, similarly to the snake that adapts its skeleton to ingest large preys, a *snake stent* would have the ability to adapt to the enlarging artery as the child grows. A computer aided drawing (CAD) is shown in figure 3.1. The notches along the *ribs* will eventually act as hinges to ensure a good deployment upon balloon expansion.

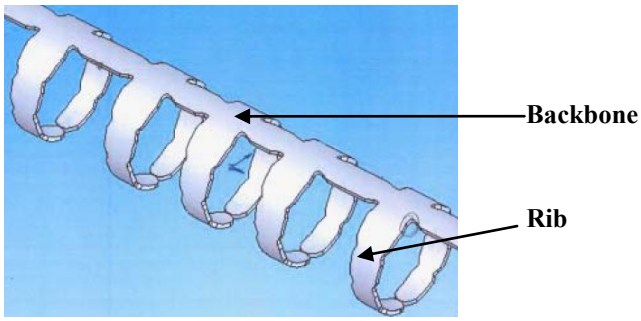

Figure 3.1: Original design idea for the pediatric stent

The design above was the starting basis for a final year project in mechanical engineering in which I participated. As mentioned, a new stent based on the snake skeleton concept has been designed and manufactured, the helical stent (figure3.2a).

For the present work, this stent is considered the first generation and the starting point for the structural design optimization. Therefore, this design will be briefly presented below.

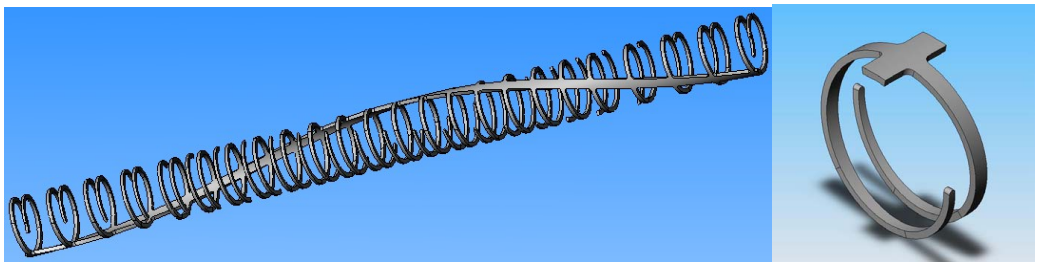

Figure 3.2: a) Helical stent b) Stent building block – One strut

First, a single building block is shown in figure 3.2b. The idea is that the backbone mainly provides structural support whereas the ribs are designed to ease deployment. In fact, they are tapered (larger at the backbone and narrower at the other end) to facilitate expansion (Figure 3.3).

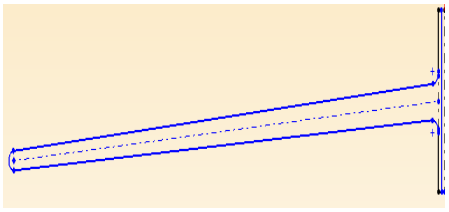

Figure 3.3: 2-D drawing of tapered rib

Moreover, the ribs were designed to have them overlapping. This is possible thanks to the angle between the rib centerline and the backbone. The overlapping allows for the possibility to cover larger diameters once expanded, as opposed to ribs that are not overlapping (Figure 3.1 vs. Figure 3.2b).

Finally, the helical backbone was meant to distribute the support along the length of the stenosis. In fact, once the stent is deployed, the ribs are not overlapping anymore and do not provide as much support as the backbone. A stent with a straight backbone (figure 3.4) would have provided increased radial support longitudinally along the same axis at the backbone location, whereas having a helical backbone distributes the support helically along the length of the artery. Figure 3.5 shows 2-D drawings of both stents. The length of the stent should be around 20mm as it is generally the length of the stenosis. Detailed dimensions are found in appendix A.

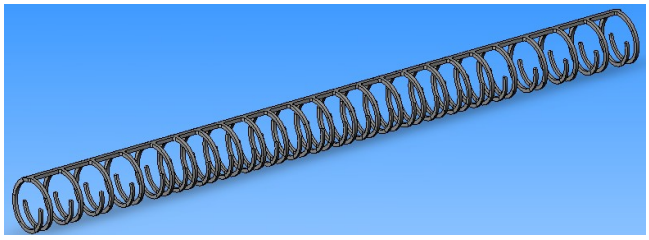

Figure 3.4: Straight backbone stent

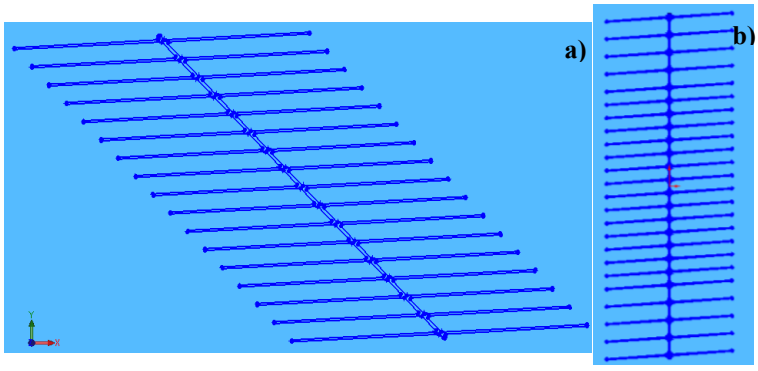

Figure 3.5: 2-D drawing of a) helical backbone stent, b) straight backbone stent

3.3. The design process

3.3.1. Generation 1 – The helical stent

As mentioned earlier, the helical stent was the starting point of the design process. The initial step for the present thesis was to test this first generation of stents. The results will be presented below as they represent the early stages of the design process.

The tests basically consisted in deploying the helical stents using angioplasty balloons to study their behaviour in free expansion (the artery's presence is not considered). Please note that when referring to balloon diameters, it is implicit that these are the final diameters once the balloons are deployed.

The undeployed outer diameter of the stent is 1.5mm. The stent was deployed on a 3mm angioplasty balloon using a balloon inflator with maximum pressures up to 30atm. The inflator and balloon are shown in figure 3.6.

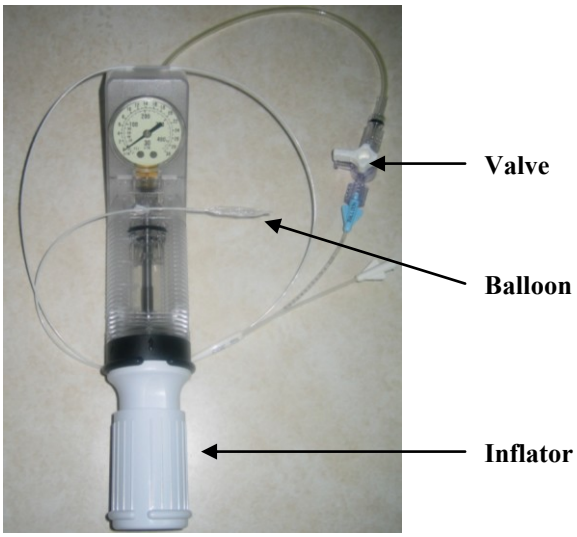

Figure 3.6: Inflator connected to an angioplasty balloon

As shown in figure 3.7, the stent deployed easily at 2.5atm, however the balloon has been inflated up to a maximal pressure of 4.5atm with no noticeable change in the stent geometry. While deflating the balloon, there seemed to be recoil unevenly distributed along the length of the stent. This could have been explained in part by how the stent easily deforms because of its small dimensions. Some struts followed correctly the deflation of the balloon.

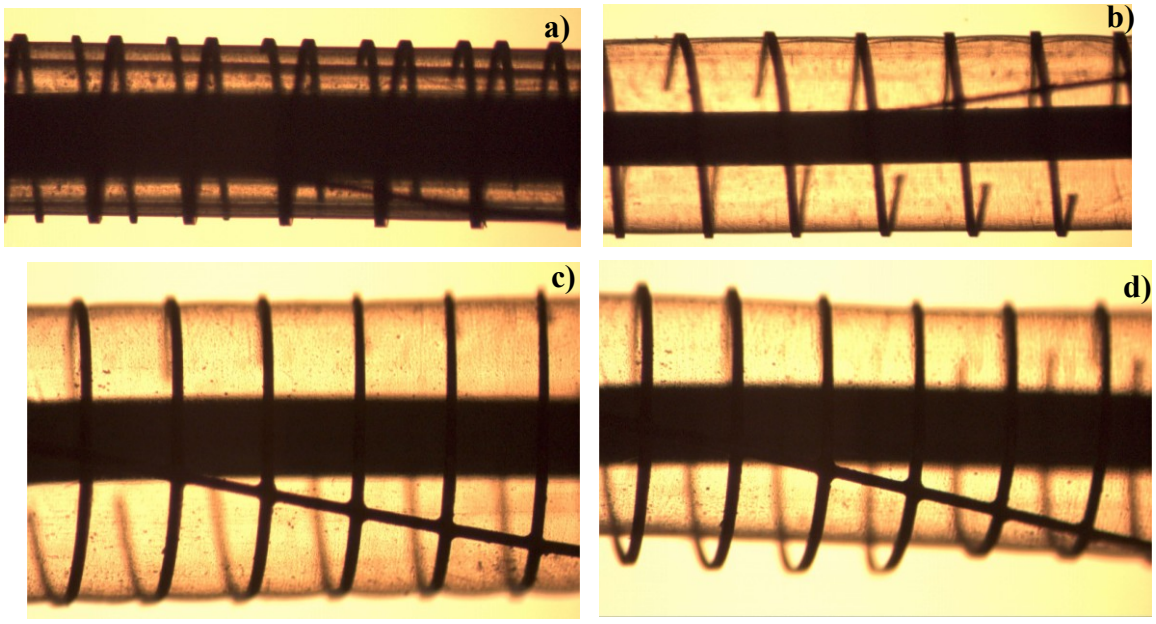

Figure 3.7: Helical stent deployed at a) 1atm b) 2.5atm c) 4.5 atm d) During balloon deflation

Figure 3.8: Helical stent a) deployed at 3mm b) Red arrows show hinge points along ribs

Moreover, the development of *hinge points* along the ribs can be noticed (figure 3.8b). The stent was designed with small notches at the backbone/rib intersection to facilitate the deployment. However, the *additional hinge points* were located before the *intended hinge points* at the backbone/rib intersection. These could be problematic as they might weaken the stent and could lead to fatigue failure under cyclic loading in the vessels.

The stent was later deployed on 5 and 6 mm balloons with the participation of Youssef Biadillah, Eng., Baylis Medical, to observe the ability of the stent to deploy at larger diameters. In this setting, the stent was serially dilated: first, on the 3mm balloon and then on the larger diameter balloons. The helical stent tended to fly off the catheter as the final diameter was too large as compared to the nominal 1.5mm OD of the stent. Moreover, there were no physical barriers (deploying the stent within a flexible tube for example) to simulate the artery's presence and thus prevent the stent from flying off. In addition, deployment at diameters 3 to 4 times the initial

diameter made the problem of *hinge points* along the ribs more pronounced than when deploying the stent on the 3mm balloon (Figure 3.9). Moreover, when using larger diameter balloons, the stent does not adopt a circular shape upon balloon deflation and this may cause the stent to poorly adapt to the arterial wall. In addition, when deploying the stent on the 6mm balloon, it became evident that, in free expansion, the stent experiences a pronounced dogboning effect while the balloon is twisted to conform to the helical shape of the stent.

Figure 3.9: Helical stent deployed a) at 5mm b) Red arrows show hinge points along ribs

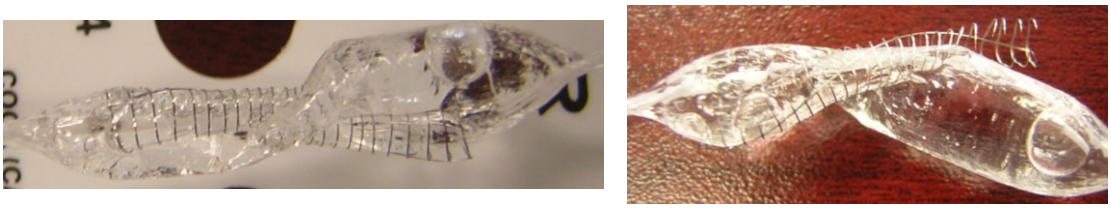

Figure 3.10: Helical stent deployed at 6mm

As pointed out by Dr. Rodés, the 1.5mm stents being too small for animal experiments, future stent generations (regardless of the design) would have to be manufactured in different size groups to accommodate patients of various ages (newborns to adolescents). The first size group is stents that would deploy to 4.5-5mm and maintain this diameter for the healing period of six months, after which the stent could be expanded to accommodate the artery growth without the need to fully cover the circumferential area of the healed artery. The stents will therefore be cut with an outer diameter of 2.3mm as it is equivalent to about 7Fr, which is the size of the sheaths used for final artery diameters of 4.5 to 5 mm.

Following the presentation of the anterior generation of stents, the design process will be described below, including the various designs studied in this project.

3.3.2. Computational models – an effective design optimization tool

Computational models provide an effective method for optimizing mechanical characteristics of a stent. In fact, it is a valuable tool to complement experimental studies, especially when these are

difficult to conduct or not feasible within a desired timeframe[117]. Moreover, it is widely accepted that Finite Element Analysis (FEA) is an efficient tool for design optimization prior to in vivo trials[118].

Therefore, in the present project, finite element packages ANSYS and ANSYS Workbench have been used in the iterative process of stent design optimization. Once the design has been modeled using the Computer Aided Design (CAD) package Solidworks, the part is imported into ANSYS and evaluated under appropriate conditions.

The deployment of a stent on a balloon is a static structural nonlinear problem. To define the problem in the ANSYS environment, a variety of data is needed. Essentially, in a FEA problem, data required includes material properties of the structure under study, boundary conditions and the loads to which the structure is subjected.

Note that stent deployment is simulated in free expansion that is the artery is not modeled in the simulations. This makes it possible to study the behaviour of the stent alone and show possible unexpected responses prior to introducing any contact analyses taking stent/artery interaction into account [119].

Moreover, the balloon has not been modelled neither. In fact, since it is much more flexible than the stent, neglecting the balloon stiffness compared to the stent stiffness is a reasonable approximation [119]. In addition, it is a realistic estimate as the stent experiences a displacement transferred from the balloon rather than a pressure.

3.3.3. Material properties, boundary conditions and loads

- **Material properties**

The stent is to be manufactured out of medical grade stainless steel 316L (SS316L). The material property, namely the stress-strain curve, has been assessed by tensile testing in our laboratory by Dr. Galaz. To describe the inelastic constitutive response of the SS316L, a *multilinear isotropic hardening* material model is used. This model uses an associative flow rule (f=q), with a von Mises/Hill criterion and isotropic hardening.

Below the SS 316L properties:

Mass density: $\rho = 7.833\times10^{-6}$ kg/m^3

Young's Modulus: E = 210 GPa

Yield Stress: σ_y = 400 MPa (0.02% offset)

Ultimate Tensile Stress: σ_{UTS} = 630 MPa

Poisson's ratio: $\nu = 0.3$

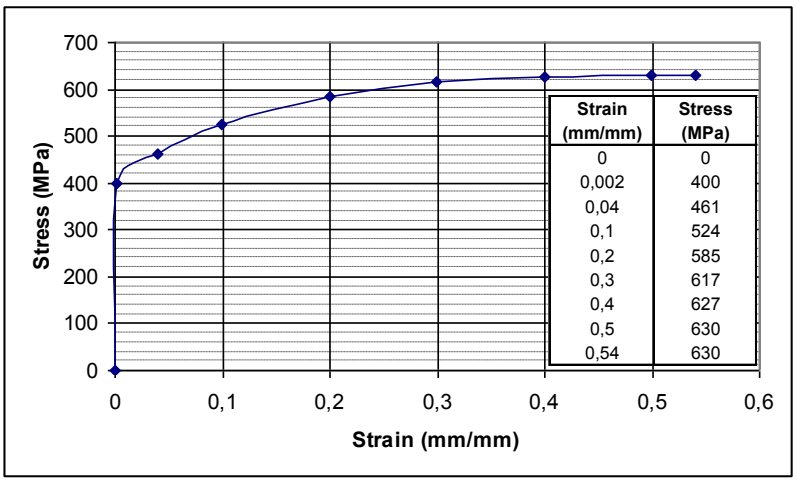

Strain (mm/mm)	Stress (MPa)
0	0
0,002	400
0,04	461
0,1	524
0,2	585
0,3	617
0,4	627
0,5	630
0,54	630

Figure 3.11: Stress-strain curve for SS316L

- **Boundary conditions**

For computational time-saving purposes, only one representative section of the stent is studied. Symmetric boundary conditions are imposed accordingly to ensure the free radial expansion of the stent [120, 121].

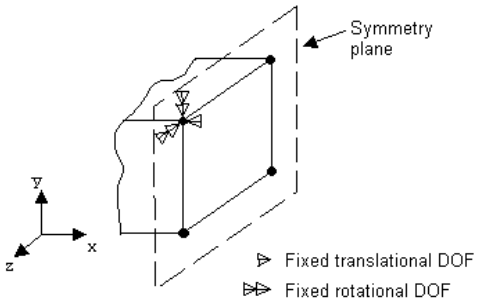

Figure 3.12: Symmetry boundary condition

Figure 3.12 describes symmetric boundary conditions: all nodes belonging to a symmetric plane are allowed to move within the plane of symmetry but not normal to the plane whereas in-plane rotations are not allowed [109].

In the simulations presented later, boundary conditions are generally applied at the two backbone ends of the segment studied (Figure 3.13)

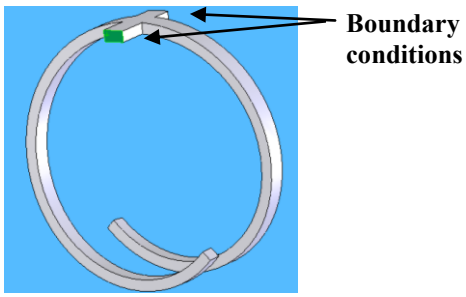

Figure 3.13: Faces on which boundary conditions are applied

- **Loads**

The literature abounds in stent expansion simulations [66, 117-126]. Depending on whether a balloon is used or not, loading varies from one author to another. In fact, either a constant pressure is applied, or pressure is linearly increased from zero to a constant value (inflation) and then linearly back to zero (deflation) to restore elastic deformation and retain plastic deformation. In other instances, a displacement is applied [117]. In fact, it is a more realistic approach as the stent really experiences a displacement transferred from the balloon upon inflation, rather than a pressure.

In the present work, pressure could not be applied along with symmetry boundary conditions. In fact, the use of symmetry BCs resulted in an under constrained model leading to rigid body motion and ultimately simulation failure. To apply pressure, a fixed support boundary condition had to be used. As a result, the obtained displacement was very small and unrealistic. Therefore, in the analyses presented below, symmetry boundary conditions are used along with an applied displacement of 0.25mm as a starting point which, in all cases, rendered a satisfactory approximation to the studied problem.

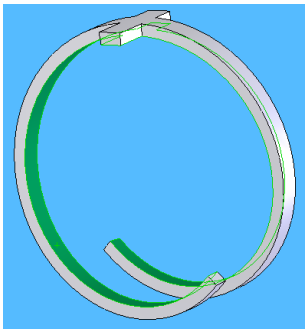

Figure 3.14: Inner surface of the stent on which displacement is applied

- **Meshing and elements**

The stent was meshed using 3-D 20-node brick structural solid element (SOLID187). It can tolerate irregular shapes and has plasticity, large deflection and large strain capabilities.

Initially, a relatively coarse mesh is used and a first simulation is run using a *strucutal error* tool. This tool shows areas where the mesh should be refined for improved convergence. The mesh is then refined accordingly.

Evaluation of design success will be based on the ability of the modeled stent to exhibit large expansion and plastic deformation.

3.4. Generation 2 stent

The generation of stents following the helical stent generation had to keep the same design advantages, mainly the idea of distributing the support along the length of the stenosis with the helical backbone.

In the second generation, the idea was to alternate the backbone at 0 and 180^0 along the length of the stent as shown in figure 3.15b. This design has thus been named the a*lternating backbone stent*.

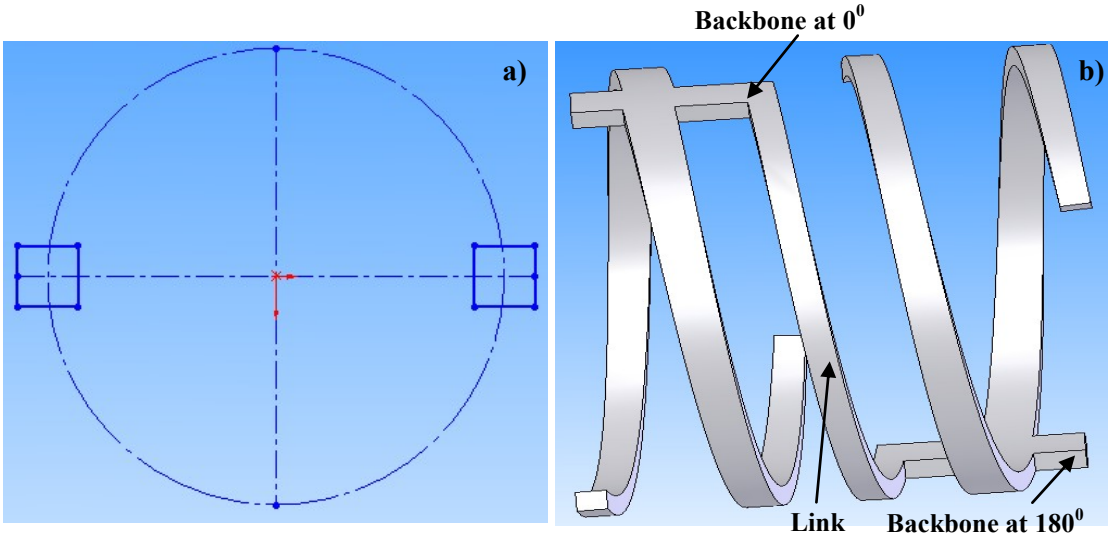

Figure 3.15: a) Alternating backbones viewed from top b) Stent

The alternating backbones are connected using a link. As in the previous design, the link and struts are drawn at an angle to allow for overlapping struts and thus offer a greater coverage of the artery at large diameters. The struts are tapered to facilitate expansion. As suggested by Dr. Mongrain, the new addition in this design is the use of *anchoring discs* at the end of the rib. The goal is to promote good endothelialisation for the stent to be well anchored in the artery and facilitate the expansion with somatic growth.

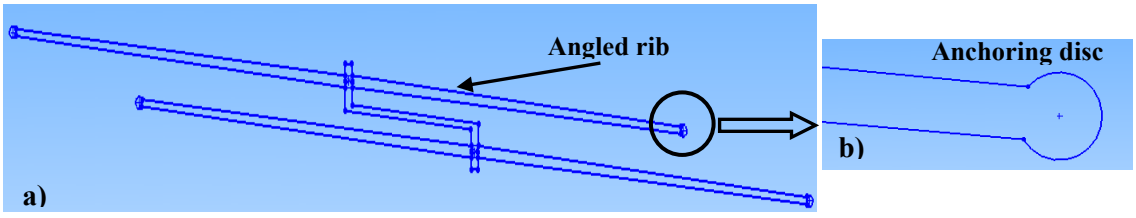

Figure 3.16: a) 2-D drawing of the alternating backbone stent b) anchoring disc

The stent has been manufactured with longer overlapping struts to allow for greater coverage when deployed at large diameters. Drawings with detailed stent dimensions are presented in appendix A.

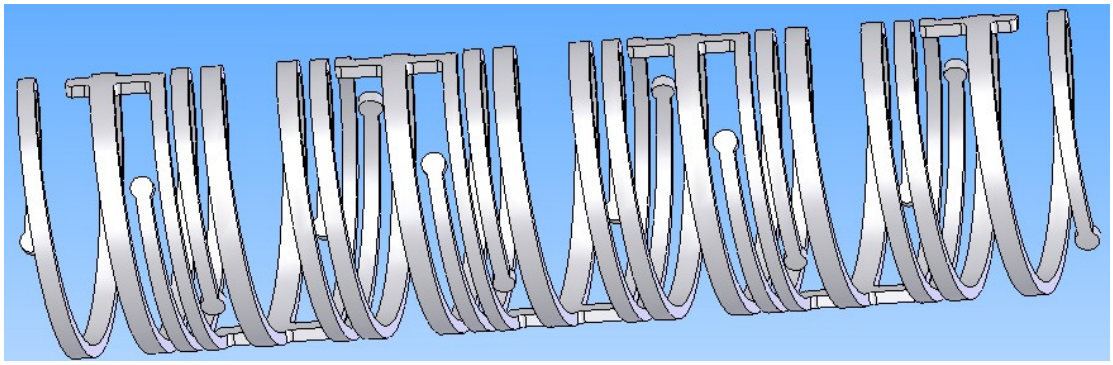

Figure 3.17: Alternating backbone stent with overlapping struts

3.4.1. Numerical results

As a starting point, simulations have been conducted on a simplified version of the stent. One ring with the link and struts having a small overlap is considered. Results are shown below.

Please note that fillets and rounds are not modeled in all simulations as this will result in longer running times.

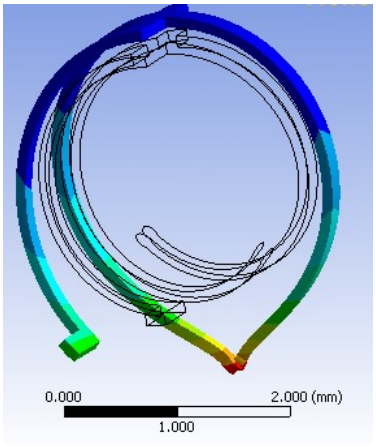

Figure 3.18: A single ring and link – applied displacement 0.25mm

It can be seen in this simplified version of the stent that the link does not seem to pose a problem as to stent deployment. The struts ends on the other hand intersect preventing the stent from fully deploying. However, one must keep in mind that the balloon has been neglected here and its presence would have helped the struts deploy in a circular rather than an oval shape.[‡]

[‡] Similar behaviour has been noticed in helical stent simulations. However, when deployed on the balloon, the struts did not collide as predicted by the simulations.

The next step is to consider two rings to evaluate how the link effectively affects deployment. In the first stages of deployment (at 38% of the load step), the stent seems to be expanding into the desired circular shape. However, as the analysis progresses (at 48% and 62% of the load step), the link piece gets irregularly deformed and leads to struts intersection. (Figure 3.19)

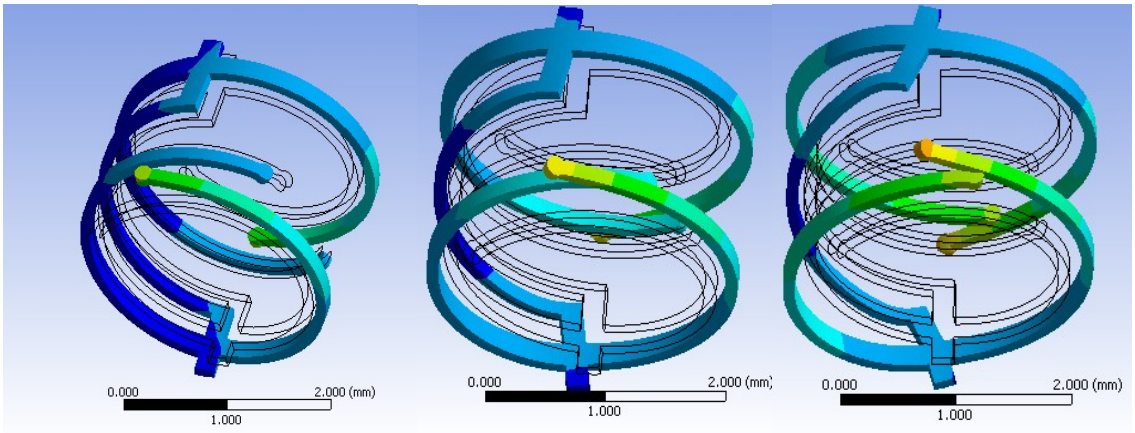

Figure 3.19: Two rings with small overlap, a) at 38% b) at 48% c) at 62% of load step

Subsequently, struts with a more pronounced overlap have been considered as well. The struts do deploy, nevertheless as they *unroll* they are displaced along the length of the stent until they collide. Below, the results are presented for one and two rings.

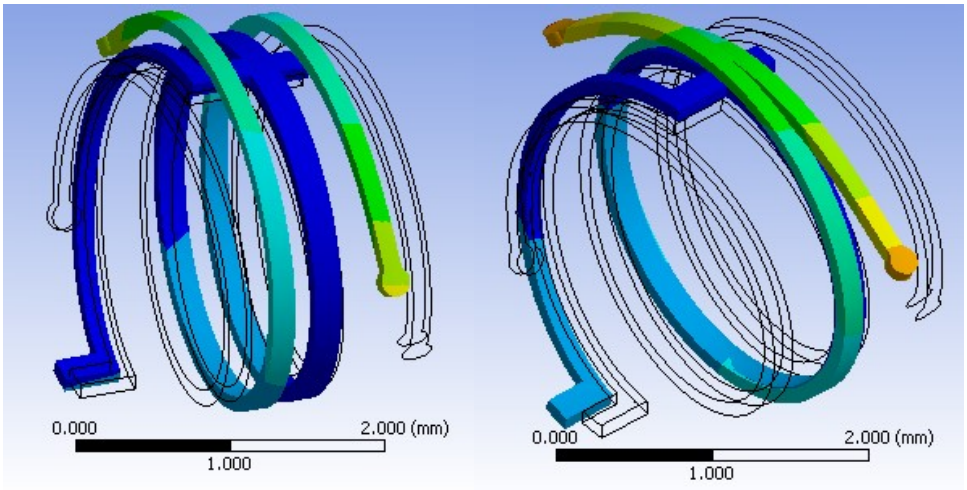

Figure 3.20: Large overlap a) 22% of load step, b) 33% of load step

Below, the simulations show the deployment of two struts. Similar behaviour is once again observed. The link is irregularly deformed and the struts collide.

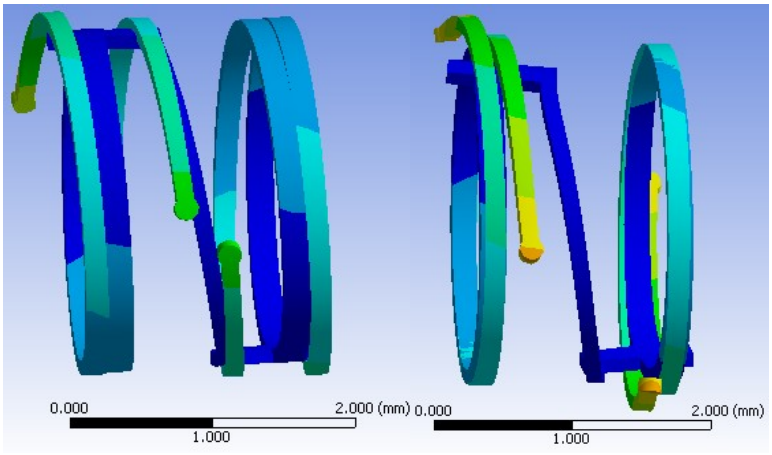

Figure 3.21: Two rings with a large overlap. Simulation at a) 20% and b) 25% of loadstep

Note that absolute displacement and von Mises stress data are not presented since the expansion is irregular and these designs will not be retained.

3.4.2. Experimental results

The next step following the simulations and prototyping of the second generation of stents is to expand them in the experimental setting. The same methodology as the one used to test the helical stent is used here. The stent is once again mounted on a balloon and expanded using the balloon inflator.

The *alternating backbone stent* failed to deploy even at the highest possible pressure. Prior to deployment under the microscope, some geometrical irregularities could be noticed. In fact, the struts seemed to be very close to each other and the diameter was not constant along the length of the stent. (Figure 3.22)

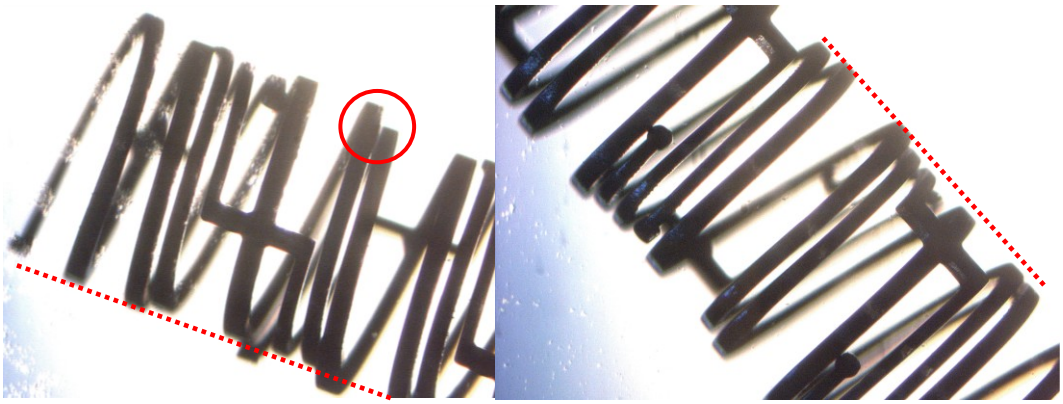

Figure 3.22: Irregular diameter prior to expansion – Shown by dashed lines

Upon deployment, it could be noticed that the struts get intertwined at the extremities of the stent (Figure 3.23). Under the assumption that it could have been the result of a wrong manipulation while mounting the stent on the balloon, the deployment has been reattempted. However, the situation would be reproduced.

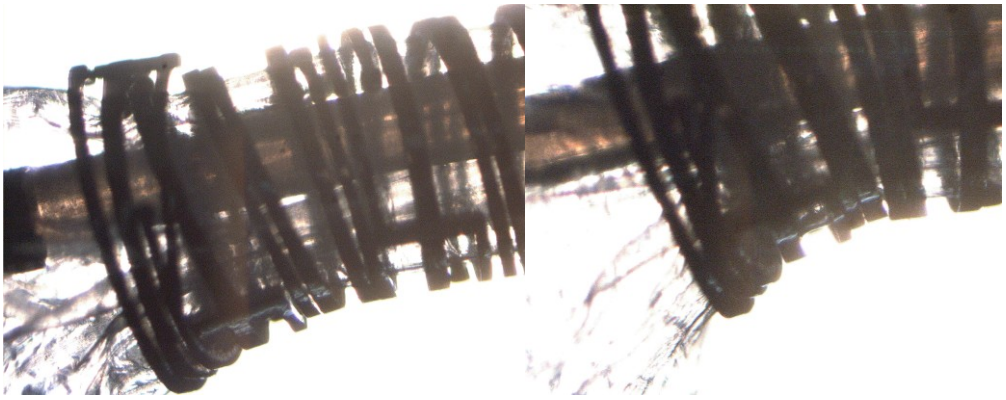

Figure 3.23: Struts at the extremities intertwine upon expansion

It was later tried to deploy the stent using a high pressure inflator with no success. The failure of this stent to deploy is a consequence of the large overlap of the struts and their proximity which leads to their interlacing. These results are coherent with the simulations results presented earlier.

3.5. Current generation (Generation 3) of stents

In the following generation of stents, the goal was to revisit the alternating backbone idea while improving expansion.

In this design, alternate backbone pieces will not be connected using a link as in the previous generation. Instead, the backbones will be in the continuity of the struts as shown in the 2-D drawing below.

The stent is cut in a 2.3mm OD cylinder with a 0.1mm wall thickness. A detailed drawing presenting the main dimensions and including all rounds and fillets is found in appendix A.

Stent dimensions have been adjusted to allow stent modelling without having ribs and backbone pieces intersecting and to obtain a reasonable number of struts along the length of the stent (Appendix A).

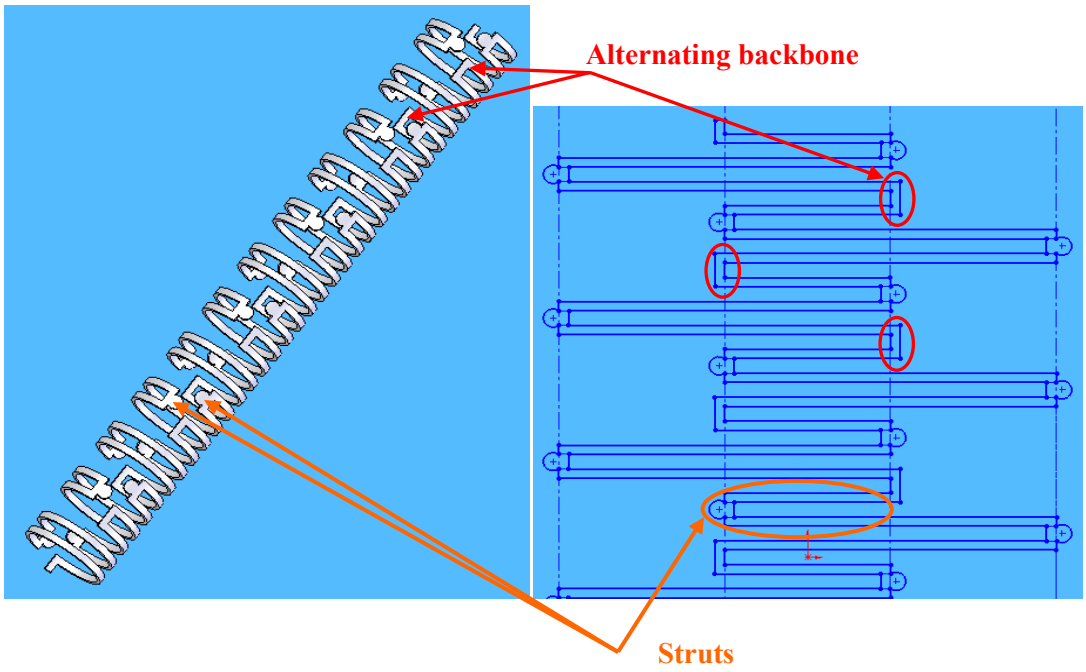

Figure 3.24: 2-D and 3-D representation of generation 3 of stents

3.5.1. Numerical results

Similarly to the previous design, only one ring is studied at first. As explained earlier a 0.25mm displacement was applied on the internal surface of the ring. The stent greatly expanded to a near circular shape with the largest expansion being at the end of the struts with a value of 1,35mm. As for plastic deformation, the stent was not plastically deformed throughout the geometry. In fact, even though the maximum von Mises stress, located at the end of the longer rib, is about

500MPa the stent does not experience stresses larger than 420-430 MPa in other areas of the ring. (Figure 3.26)

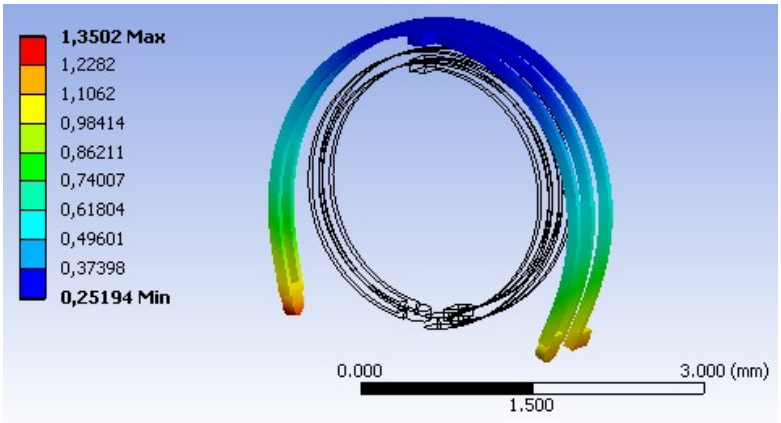

Figure 3.25: Total deformation (mm) in a single ring – Load: 0.25mm

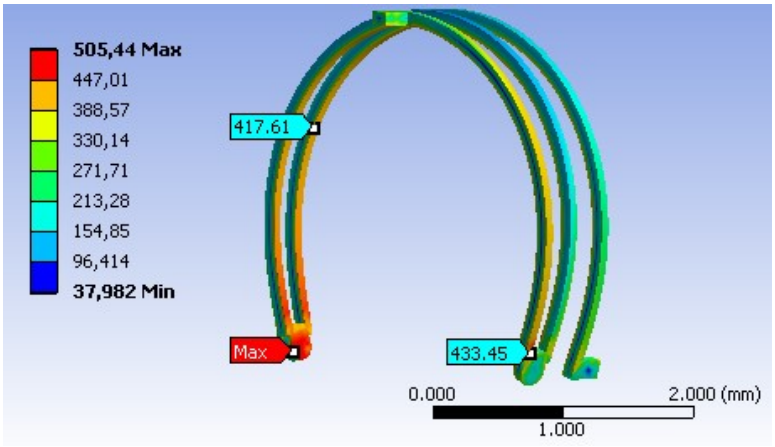

Figure 3.26: Equivalent von Mises stress (MPa) in a single ring – Displacement: 0.25mm

Since the ultimate tensile stress has not been reached and in order to evaluate the ability of the stent to deploy at higher diameters, a displacement of 0.35mm has been simulated as well. Again, the stent expanded into a near circular shape (Figure 3.27 – The wireframe represents the undeployed stent). However, one of the segments deployed in an uneven fashion (Figure 3.28). Moreover, ultimate tensile stress has almost been reached (maximum of about 617MPa at the end of the longest strut). The strut seems to be plastically deformed with stresses generally varying from about 450 to 550 MPa.

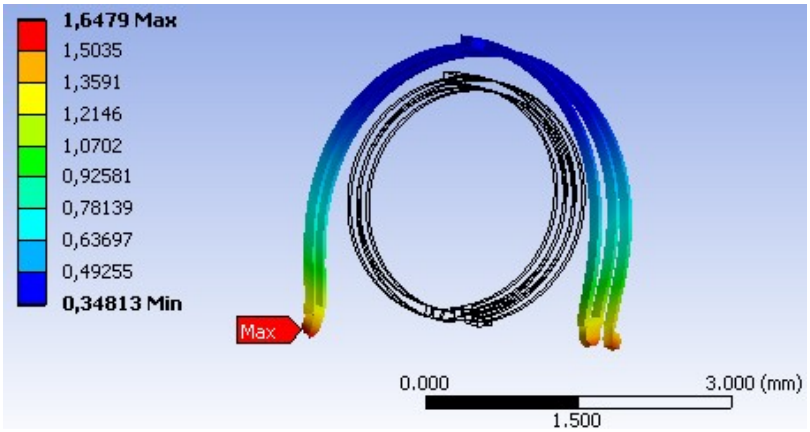

Figure 3.27: Total deformation (mm) in a single ring – Load: 0.35mm

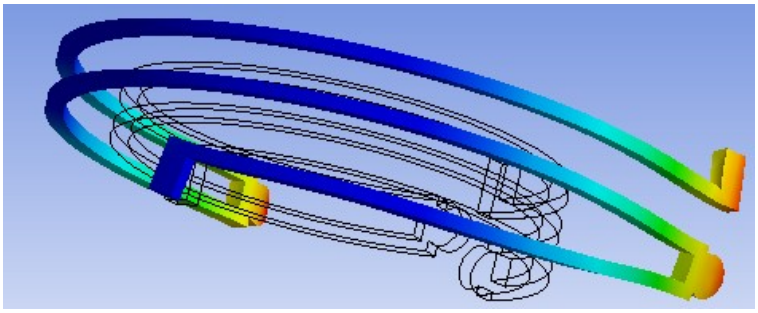

Figure 3.28: Irregular deployment at 0.35mm

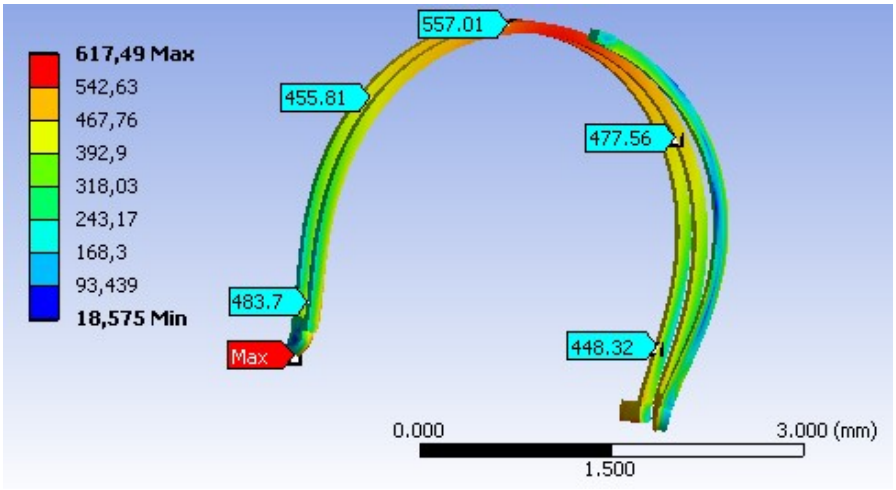

Figure 3.29: Equivalent von Mises stress (MPa) in a single ring – Load: 0.35mm

As for the previous generation, the next simulation analyzed two rings of the stent. When 0.25mm displacement has been applied, the stent expanded similarly to one ring until 49% of the load step (Figure 3.30). After that, parts of the stent translated along the Z-axis resulting in an irregular shape (Figure 3.31). Moreover, although the maximum stress is 509MPa, the stent is not completely deformed in the plastic regime (stresses vary between 410 and 430 MPa along the struts)

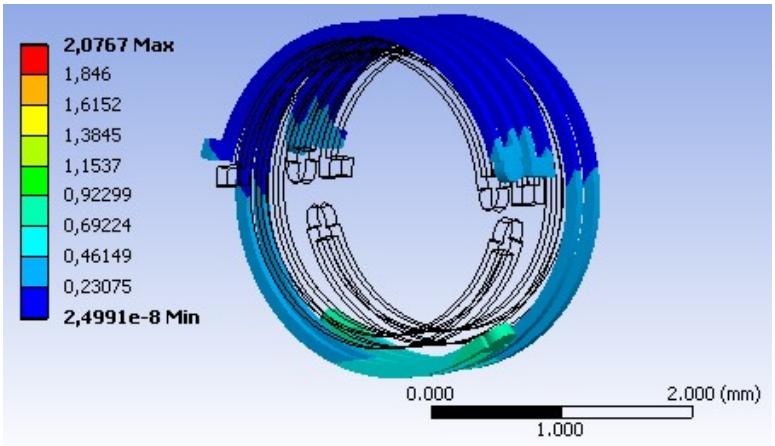

Figure 3.30: Total deformation (mm) in two rings – 49% of load step

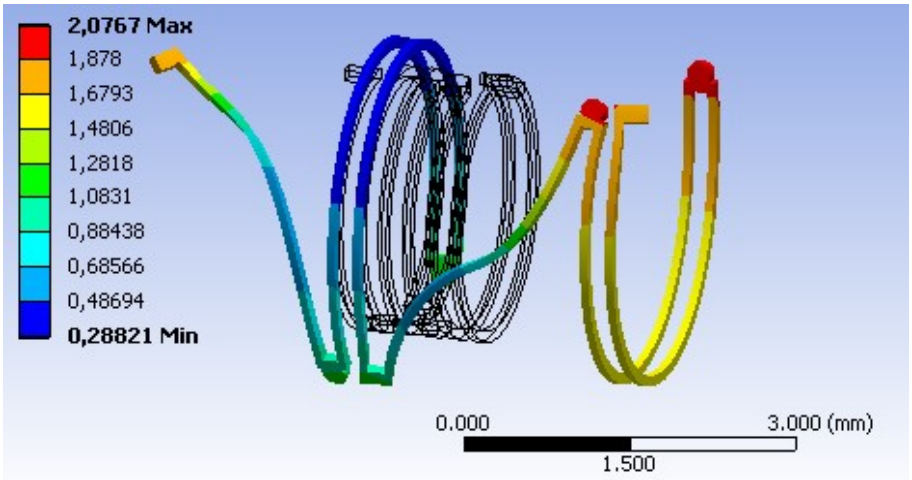

Figure 3.31: Total deformation (mm) in two rings

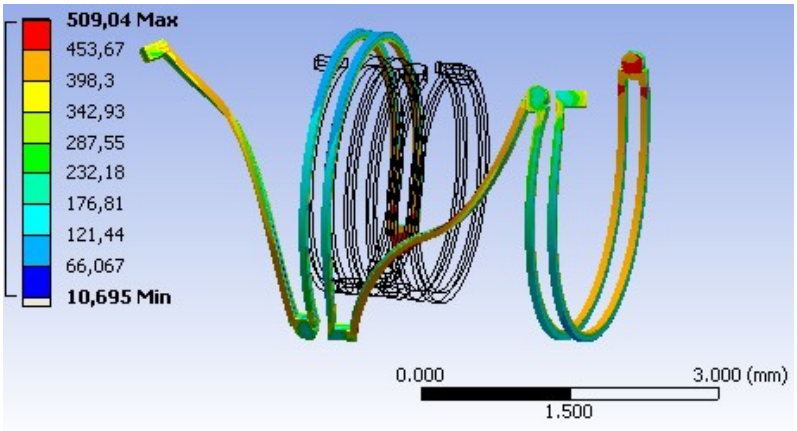

Figure 3.32: Equivalent von Mises stress (MPa)in two rings

Finally, six rings have been analyzed to verify if the behaviour is reproducible for a larger portion of the stent. The same scenario recurred: the stent deployed evenly until 47% of the loadstep

(Figure 3.33) after which the deformation becomes irregular (Figure3.34). Again, the stent is plastically deformed only in some sections of the stent. (Figure 3.35)

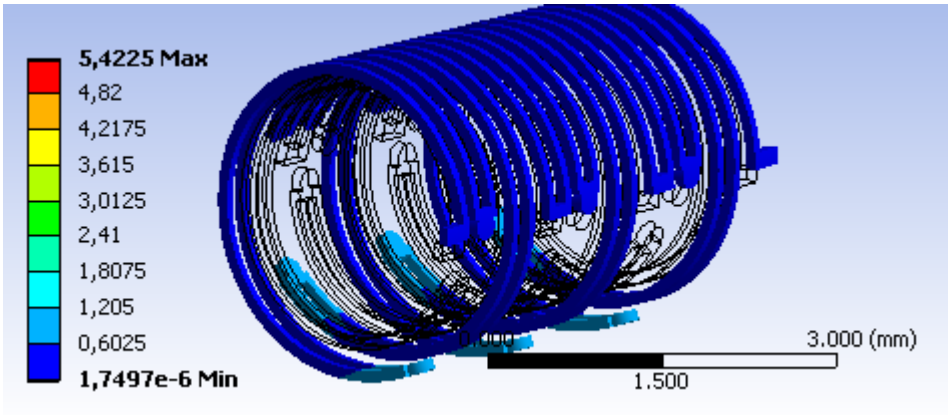

Figure 3.33: Total deformation (mm) in six rings – 47% of load step

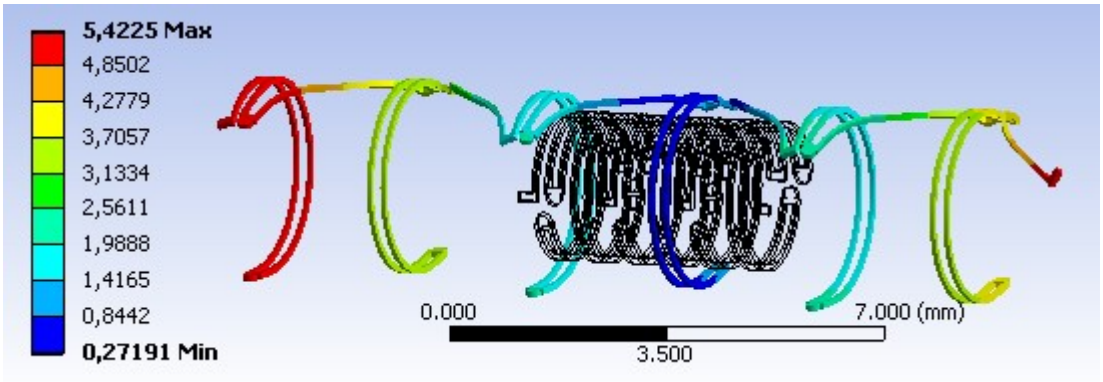

Figure 3.34: Total deformation (mm) in six rings

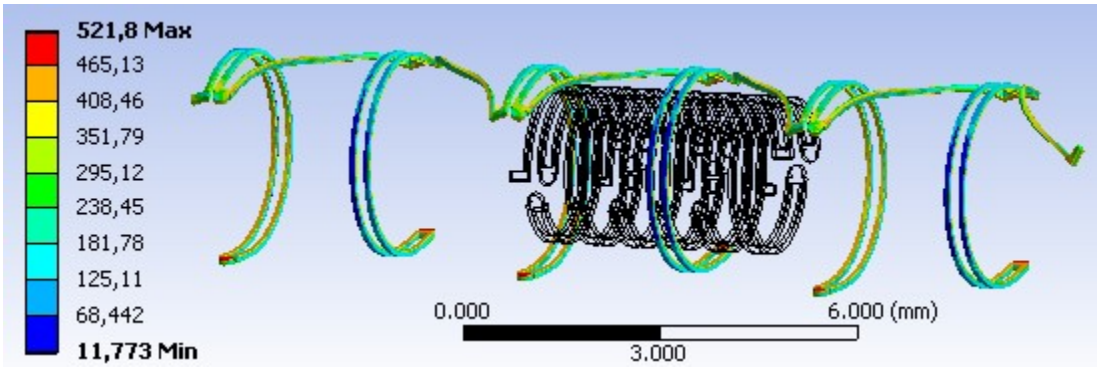

Figure 3.35: Equivalent von Mises stress (MPa)in six rings

3.5.2.Testing results

The generation 3 of stents is deployable at pressures of about 1 to 1.5 atm. Figure 3.22 shows the stent during deployment on a 5mm balloon. It can be seen that the distal struts slowly open up as

the balloon is inflated. The central struts then follow. Because of this dogboning effect, the distal struts are more deformed than the central portion of the stent.

Figure 3.36: Expansion of the generation 3 stent on a 5mm balloon

Upon balloon removal, it is possible to observe that the stent behaves like a straight backbone stent (presented in section 3.2). In fact, the shorter struts seem to behave as one large backbone while the long struts exhibit a larger expansion. (Figure 3.37) These results seem to be in accordance with numerical results presented earlier for one ring. However, the amount of translation of middle struts as shown in the simulations has not been reproduced in the experimental setting.

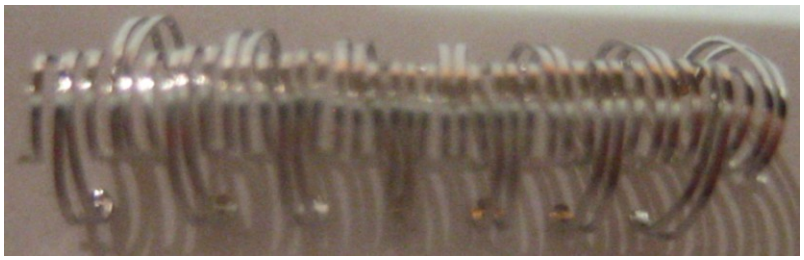

Figure 3.37: Deployed stent resembles a straight backbone stent

In order to compare this pediatric stent to adult coronary stent data, four stent specimens have been deployed and foreshortening and recoil calculated. For each stent, each measurement needed for the calculations has been measured at least three times. Pictures of the stent in various stages of the deployment are taken and the desired quantities are measured using *Adobe Photoshop*. Detailed steps and sample calculations are presented in appendix B. Table 1 below summarizes the foreshortening and recoil data for each of the four specimens.

	SPECIMEN 1				SPECIMEN 2			
	Initial length (mm)	Final length (mm)	Inflated OD (mm)	Final OD (mm)	Initial length (mm)	Final length (mm)	InflatedOD (mm)	Final OD (mm)
#1	17,29	16,23	5,0	4,56	21,07	17,67	5,0	4,48
#2	17,73	15,9		4,60	21,16	17,57		4,43
#3	17,80	14,75		4,58	21,13	17,61		4,45
Δ	17,61	15,63		4,58	21,12	17,62		4,45
	Foreshortening (%)		Recoil (%)		Foreshortening (%)		Recoil (%)	
	11,2		8,4		16,6		10,9	
	SPECIMEN 3				SPECIMEN 4			
	Initial length (mm)	Final length (mm)	Inflated OD (mm)	Final OD (mm)	Initial length (mm)	Final length (mm)	Inflated OD (mm)	Final OD (mm)
#1	21,9	18,72	5,0	4,64	21,22	18,79	5,0	4,82
#2	21,4	18,82		4,41	20,96	18,66		4,46
#3	21,50	18,77		4,48	21,08	18,81		4,83
Δ	21,60	18,77		4,51	21,09	18,75		4,70
	Foreshortening (%)		Recoil (%)		Foreshortening (%)		Recoil (%)	
	13,1		9,8		11,1		5,9	

Average FS	Average recoil
13,0%	8,8%

Table 3.1: Foreshortening and recoil data for generation 3 stents

The initial and final lengths are measured when the stent is unexpanded and deployed respectively. Inflated OD is the inflated outer diameter when the balloon is at its maximum diameter. Finally, the final OD is the measured outer diameter upon balloon removal.

The test results above, for the third generation of stents, are satisfactory as it is a first iteration of this particular design. In fact, foreshortening of 13% (<20%) and a small amount of recoil of 8.8% was achieved. In addition, it was possible to expand the stent to more than twice its original outer diameter (from to 2.3mm to 5mm). Finally, the stent satisfies the requirement of flexibility as well (figure 3.38).

Figure 3.38: Flexed undeployed stent

4. Conclusion

4.1. Limitations and future research

In general, the simulations conducted in the course of this project offer a reasonable approximation to the real life scenario. However, several limitations exist. In fact, since the balloon is not included in the model, effects such as dogboning could not be reproduced numerically. Moreover, foreshortening could not be assessed as only portions of the stent are studied. Moreover, the displacement only simulates the inflation phase of the balloon. Recoil could not be calculated neither since the smallest total displacement is equivalent to the applied displacement.

As for the experiments, the main limitations are related to the stents size. Effectively, since the stents are very small, a wrong manipulation can easily lead to an undesirable stent deformation. In addition, calculated values in the previous section are affected by user error. In fact, measured values using *Adobe Photoshop* are approximate since they depend on the user's ability to precisely calibrate the desired quantities in the picture.

Another major limitation in the design process is the prototyping process. In fact, the design is laser cut vertically onto the steel tube. Therefore, the stent design has to be drawn in a 2-D closed contour drawing. This must be considered while developing design ideas.

Concerning the current generation of stents, even if it is a satisfactory first iteration of the design, various improvements could be made. Indeed, since the stent behaves similarly to a straight backbone stent, the shorter struts could be made longer as a first step. Moreover, since the current design does not have overlapping ribs, these could be added in a next iteration. (Figures 4.1, 4.2)

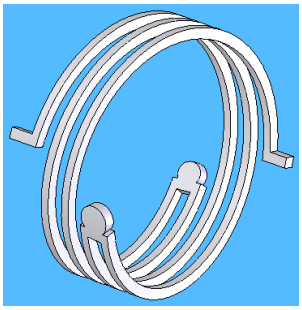

Figure 4.1: Modified g*eneration 3* ring with overlap and longer strut

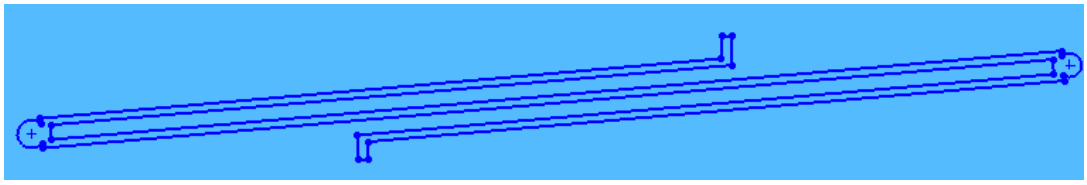

Figure 4.2: 2-D drawing of modified *generation 3* ring with overlap and longer strut

Also, it should be considered to laser cut the stent out of a slightly thicker tube to maintain flexibility and ease of deployment while offering a more *robust* stent. Stent current dimensions including strut thickness and width for example could be tuned as well. The distal struts could be reinforced as well to minimize the irregular deformation at the beginning of the inflation phase. Serial dilation could be tried as well to verify if it would allow the distal ends of the stent to deploy gradually.

Figure 4.3: Draft idea to reinforce distal struts

Future work would therefore include improving the current stent design. Another aspect to be considered is studying the fatigue life of the stent. In fact, since the endoprosthesis is in a high cycle fatigue environment, it is fundamental that it withstands the cyclic stresses.

4.2. Concluding remarks

Motivated by the need for a pediatric stent specifically designed for children, this study presents the iterative design process by which a pediatric stent has been structurally optimized. Mainly, the design process consisted of modeling the stent design concepts using CAD software, simulating its expansion under various boundary and loading conditions using a FE package, to finally perform tests in free expansion.

Although limitations exist, the current generation of stents rendered satisfactory results as for deployment, plastic deformation, foreshortening, recoil, and other design criteria. While this design needs further improvements, it constitutes a reasonable fulfillment of the objectives.

References

1. *Anatomy of the human heart*. January 6, 2009]; Available from: http://www.texasheartinstitute.org/HIC/anatomy/Anatomy.cfm.
2. *Heart valves*. January 6, 2009]; Available from: http://www.americanheart.org/presenter.jhtml?identifier=4598.
3. *Your Heart valves*. January 6, 2009]; Available from: http://www.clevelandclinic.org/heartcenter/pub/guide/disease/valve/yourheartvalves.htm.
4. *Artery*. January 6, 2009]; Available from: http://ljk.imag.fr/membres/Christophe.Prudhomme/images/artery.jpg.
5. *Material properties of arterial layers*. January 6, 2009]; Available from: http://www.csm.ornl.gov/Internships/rams_06/websites/e_lennartz/Materialprop.htm.
6. *Cardiovascular disorders - Pulmonary stenosis*. January 6, 2009]; Available from: http://www.hsc.virginia.edu/uvahealth/peds_cardiac/ps.cfm.
7. *Pulmonary stenosis*. January 6, 2009]; Available from: http://childrensnyp.org/mschony/P01815.html.
8. Trivedi, K.R. and L.N. Benson, *Interventional strategies in the management of peripheral pulmonary artery stenosis.* J Interv Cardiol, 2003. **16**(2): p. 171-88.
9. Mullins, C.E., et al., *Implantation of balloon-expandable intravascular grafts by catheterization in pulmonary arteries and systemic veins.* Circulation, 1988. **77**(1): p. 188-99.
10. Bacha, E.A. and J. Kreutzer, *Comprehensive management of branch pulmonary artery stenosis.* J Interv Cardiol, 2001. **14**(3): p. 367-75.
11. Freedom, R.M., et al., eds. *The natural and modified history of congenital heart disease*. 2003, Wiley-Blackwell. 904.
12. Benson, L.N., D. Nykanen, and R.M. Freedom, *Endovascular stents in congenital heart disease.* Prog Cardiovasc Dis, 1996. **39**(2): p. 165-86.
13. Mullins, C.E., ed. *Cardiac catheterization in congenital heart disease*. 2005, Wiley-Blackwell. 944.
14. Chau, A.K. and M.P. Leung, *Management of branch pulmonary artery stenosis: balloon angioplasty or endovascular stenting.* Clin Exp Pharmacol Physiol, 1997. **24**(12): p. 960-2.
15. Chau, A., *Stent Implantation in Congenital Heart Disease: A New Therapeutic Modality. HK J Paediatr (new series)*, 2005. **10**: p. 286-298.

16. Lock, J.E., et al., *Transvenous angioplasty of experimental branch pulmonary artery stenosis in newborn lambs.* Circulation, 1981. **64**(5): p. 886-93.
17. Lock, J.E., et al., *Balloon dilation angioplasty of hypoplastic and stenotic pulmonary arteries.* Circulation, 1983. **67**(5): p. 962-7.
18. Ring, J.C., et al., *Management of congenital stenosis of a branch pulmonary artery with balloon dilation angioplasty. Report of 52 procedures.* J Thorac Cardiovasc Surg, 1985. **90**(1): p. 35-44.
19. *Cardiac catherization (angioplasty)*. December 17, 2008]; Available from: http://redseaheartcenter.com/Procedure%20Cardiac%20Catherization%20(angioplasty).html.
20. *Percutaneous angioplasty*. December 17, 2008]; Available from: http://www.medtek.ki.se/medicaldevices/album/Ch%2011%20Tissues%20and%20calculi/slides/F%2011-13%20Percutaneous%20angioplasty.html.
21. Rocchini, A.P. and D. Kveselis, *The use of balloon angioplasty in the pediatric patient.* Pediatr Clin North Am, 1984. **31**(6): p. 1293-305.
22. Rocchini, A.P., et al., *Use of balloon angioplasty to treat peripheral pulmonary stenosis.* Am J Cardiol, 1984. **54**(8): p. 1069-73.
23. Okubo, M. and L.N. Benson, *Intravascular and intracardiac stents used in congenital heart disease.* Curr Opin Cardiol, 2001. **16**(2): p. 84-91.
24. Cheatham, J.P., *Improved stents for pediatric applications.* Prog Pediatr Cardiol, 2001. **14**(1): p. 95-115.
25. Palmaz, J.C., et al., *Expandable intrahepatic portacaval shunt stents: early experience in the dog.* AJR Am J Roentgenol, 1985. **145**(4): p. 821-5.
26. Palmaz, J.C., et al., *Atherosclerotic rabbit aortas: expandable intraluminal grafting.* Radiology, 1986. **160**(3): p. 723-6.
27. Palmaz, J.C., et al., *Expandable intrahepatic portacaval shunt stents in dogs with chronic portal hypertension.* AJR Am J Roentgenol, 1986. **147**(6): p. 1251-4.
28. Palmaz, J., et al., *Intraluminal Palmaz stent implantation. The first clinical case report on a balloon-expanded vascular prosthesis.* Radiologe, 1987. **27**(12): p. 560-563.
29. Palmaz, J.C., et al., *Intraluminal stents in atherosclerotic iliac artery stenosis: preliminary report of a multicenter study.* Radiology, 1988. **168**(3): p. 727-731.
30. Schatz, R.A., et al., *Balloon-expandable intracoronary stents in the adult dog.* Circulation, 1987. **76**(2): p. 450-7.

31. Olaughlin, M.P., et al., *Use of endovascular stents in congenital heart disease.* Circulation, 1991. **83**(6): p. 1923-1939.
32. Ing, F., *Stents: what's available to the pediatric interventional cardiologist?* Catheter Cardiovasc Interv, 2002. **57**(3): p. 374-86.
33. van Gameren, M., et al., *Early complications of stenting in patients with congenital heart disease: a multicentre study.* Eur Heart J, 2006. **27**(22): p. 2709-15.
34. O'Laughlin, M.P., et al., *Implantation and intermediate-term follow-up of stents in congenital heart disease.* Circulation, 1993. **88**(2): p. 605-14.
35. Hijazi, Z.M., et al., *Stent implantation for relief of pulmonary artery stenosis: immediate and short-term results.* Cathet Cardiovasc Diagn, 1996. **38**(1): p. 16-23.
36. Hatai, Y., et al., *Endovascular stents in children under 1 year of age: acute impact and late results.* Br Heart J, 1995. **74**(6): p. 689-95.
37. Fogelman, R., et al., *Endovascular stents in the pulmonary circulation. Clinical impact on management and medium-term follow-up.* Circulation, 1995. **92**(4): p. 881-5.
38. O'Laughlin, M.P., *Catheterization treatment of stenosis and hypoplasia of pulmonary arteries.* Pediatric Cardiology, 1998. **19**(1): p. 48-56.
39. Saidi, A.S., et al., *Balloon pulmonary valvuloplasty and stent implantation for peripheral pulmonary artery stenosis in Alagille syndrome.* Texas Heart Institute Journal, 1998. **25**(1): p. 79-82.
40. Morrow, W.R., et al., *Balloon angioplasty with stent implantation in experimental coarctation of the aorta.* Circ., 1994. **89**(6): p. 2677-2683.
41. Ing, F.F., et al., *Arterial stents in the management of neurofibromatosis and renovascular hypertension in a pediatric-patient - case-report of a new treatment modality.* Cardiovasc Intervent Radiol, 1995. **18**(6): p. 414-418.
42. Ruiz, C.E. and H.P. Zhang, *Stenting coarctation of the aorta: Promising concept but primitive technology.* Catheter and Cardiovasc Diagnosis, 1996. **39**(1): p. 43-43.
43. Ovaert, C., et al., *Transcatheter treatment of coarctation of the aorta: A review.* Pediatr Cardiol, 1998. **19**(1): p. 27-44.
44. D'Souza, S.J.A., et al., *Diagnosis and management of stenotic aorto-arteriopathy in childhood.* Journal of Pediatrics, 1998. **132**(6): p. 1016-1022.
45. *Managing risky conditions*. December 17, 2008]; Available from: http://www.theuniversityhospital.com/stroke/risky.htm.
46. Lumsden, A.B., et al., eds. *Endovascular therapy: principles of peripheral interventions*. 2006, Wiley-Blackwell. 312.

47. Rao, P.S., *Stents in the management of congenital heart disease in pediatric and adult patients.* Indian Heart J, 2001. **53**(6): p. 714-30.
48. Cheung, Y.F., et al., *Early and intermediate-term complications of self-expanding stents limit its potential application in children with congenital heart disease.* J Am Coll Cardiol, 2000. **35**(4): p. 1007-1015.
49. Redington, A.N., J. Weil, and J. Somerville, *Self-expanding stents in congenital heart-disease.* Br Heart J, 1994. **72**(4): p. 378-383.
50. Brown, S.C., et al., *Self expandable stents for relief of venous baffle obstruction after the Mustard operation.* Heart, 1998. **79**(3): p. 230-233.
51. *Stent with balloon angioplasty*. December 17, 2008]; Available from: http://www.surgery.usc.edu/divisions/ct/graphics/stent.jpg.
52. Baerlocher, L., et al., *Stent implantation and balloon angioplasty for treatment of branch pulmonary artery stenosis in children.* Clin Res Cardiol, 2008. **97**(5): p. 310-7.
53. O'Laughlin M, P., *Balloon-expandable stenting in pediatric cardiology.* J Interv Cardiol, 1995. **8**(5): p. 463-75.
54. Weintraub, W.S., *The pathophysiology and burden of restenosis.* Am J Cardiol, 2007. **100**(5A): p. 3K-9K.
55. Rajagopal, V. and S.G. Rockson, *Coronary restenosis: a review of mechanisms and management.* Am J Med, 2003. **115**(7): p. 547-53.
56. Palmaz, J.C., *Intravascular stents: tissue-stent interactions and design considerations.* AJR Am J Roentgenol, 1993. **160**(3): p. 613-8.
57. Tomita, H., et al., *Late neointimal proliferation following implantation of stents for relief of pulmonary arterial stenosis.* Cardiol Young, 2002. **12**(2): p. 125-9.
58. Duke, C., E. Rosenthal, and S.A. Qureshi, *The efficacy and safety of stent redilatation in congenital heart disease.* Heart, 2003. **89**(8): p. 905-12.
59. Shaffer, K.M., et al., *Intravascular stents in congenital heart disease: short- and long-term results from a large single-center experience.* J Am Coll Cardiol, 1998. **31**(3): p. 661-7.
60. Mauro, M.A., *The battle of intimal hyperplasia in the war against femoropopliteal disease.* Radiology, 2004. **231**(2): p. 299-301.
61. Breinholt, J.P., et al., *Stent fractures in congenital heart disease.* Catheter Cardiovasc Interv, 2008. **72**(7): p. 977-82.

62. McMahon, C.J., et al., *Refinements in the implantation of pulmonary arterial stents: impact on morbidity and mortality of the procedure over the last two decades.* Cardiol Young, 2002. **12**(5): p. 445-52.
63. Ing, F.F., et al., *Repeat dilation of intravascular stents in congenital heart defects.* Circulation, 1995. **92**(4): p. 893-7.
64. McMahon, C.J., et al., *Redilation of endovascular stents in congenital heart disease: factors implicated in the development of restenosis and neointimal proliferation.* J Am Coll Cardiol, 2001. **38**(2): p. 521-6.
65. Schneider, M., et al., *Various reasons for repeat dilatation of stented pulmonary arteries in pediatric patients.* Heart, 2002. **88**(5): p. 505-509.
66. Wang, W.Q., et al., *Analysis of the transient expansion behavior and design optimization of coronary stents by finite element method.* J Biomech, 2006. **39**(1): p. 21-32.
67. Turner, D.R., et al., *Initial experience using the Palmaz Corinthian stent for right ventricular outflow obstruction in infants and small children.* Catheter Cardiovasc Interv, 2000. **51**(4): p. 444-9.
68. Pass, R.H., et al., *Endovascular stent implantation in the pulmonary arteries of infants and children without the use of a long vascular sheath.* Catheter Cardiovasc Interv, 2002. **55**(4): p. 505-9.
69. Bergersen, L. and J.E. Lock, *What is the current option of first choice for treatment of pulmonary arterial stenosis?* Cardiol Young, 2006. **16**(4): p. 329-38.
70. Forbes, T.J., et al., *The Genesis stent: A new low-profile stent for use in infants, children, and adults with congenital heart disease.* Catheter Cardiovasc Interv, 2003. **59**(3): p. 406-14.
71. Rutledge, J.M., et al., *Initial experience with intratherapeutics Intrastent Doublestrut LD stents in patients with congenital heart defects.* Catheter Cardiovasc Interv, 2002. **56**(4): p. 541-8.
72. Recto, M.R. and R.G. Grifka, *IntraStent double-strut LD: collapse and recoil following use in postoperative stenoses.* Catheter Cardiovasc Interv, 2002. **56**(2): p. 254-61.
73. *CP Stent*. January 6, 2009]; Available from: http://www.numedforchildren.com/cpstent-ce.htm.
74. Ewert, P., et al., *The CP stent--short, long, covered--for the treatment of aortic coarctation, stenosis of pulmonary arteries and caval veins, and Fontan anastomosis in children and adults: an evaluation of 60 stents in 53 patients.* Heart, 2005. **91**(7): p. 948-53.

75. Ewert, P., et al., *Novel growth stent for the permanent treatment of vessel stenosis in growing children: an experimental study.* Catheter Cardiovasc Interv, 2004. **62**(4): p. 506-10.
76. Ewert, P., et al., *Early and mid-term results with the Growth Stent--a possible concept for transcatheter treatment of aortic coarctation from infancy to adulthood by stent implantation?* Catheter Cardiovasc Interv, 2008. **71**(1): p. 120-6.
77. Ing, F.F., et al., *A new "open-ring stent".* Circulation, 1996. **94**(8): p. 323-323.
78. Mullins, C.E., *Inappropriate stents: primary cause of failure of stent redilation in coarctation of the aorta.* Catheter Cardiovas Interv, 2008. **72**(4): p. 557-558.
79. Sigler, M., et al., *Breakable stent for interventions in infants and neonates: an animal study and histopathological findings.* Heart, 2006. **92**(2): p. 245-8.
80. Peuster, M., et al., *A novel approach to temporary stenting: degradable cardiovascular stents produced from corrodible metal-results 6-18 months after implantation into New Zealand white rabbits.* Heart, 2001. **86**(5): p. 563-9.
81. Duckers, H.J., E.G. Nabel, and P.W. Serruys, eds. *Essentials of Restenosis For the Interventional Cardiologist*. Contemporary Cardiology 2007, Humana Press. 458.
82. Tsuji, T., et al., *One year follow-up of biodegradable self-expanding stent implantation in humans.* J Am Coll Cardiol, 2001. **37**(2): p. 47a-47a.
83. Tsuji, T., et al., *A new biodegradable coronary stent: Acute and 3 months clinical and angiographic follow-up.* Circulation, 1999. **100**(18): p. 292-293.
84. Tamai, H., et al., *A biodegradable poly-l-lactic acid coronary stent in the porcine coronary artery.* J Interv Cardiol, 1999. **12**(6): p. 443-449.
85. Tsuji, T., et al., *Clinical and angiographic follow-up of a new biodegradable coronary stent (Igaki-Tamai stent).* J Am Coll Cardiol, 2000. **35**(2): p. 89a-89a.
86. Waksman, R., *Update on bioabsorbable stents: from bench to clinical.* J Interv Cardiol, 2006. **19**(5): p. 414-21.
87. Tamai, H., et al., *Initial and 6-month results of biodegradable poly-l-lactic acid coronary stents in humans.* Circulation, 2000. **102**(4): p. 399-404.
88. Di Mario, C., et al., *Drug-eluting bioabsorbable magnesium stent.* J Interv Cardiol, 2004. **17**(6): p. 391-5.
89. Heublein, B., et al., *Biocorrosion of magnesium alloys: a new principle in cardiovascular implant technology?* Heart, 2003. **89**(6): p. 651-6.

90. Cejna, M., et al., *Biocompatibility and performance of the wallstent and several covered stents in a sheep iliac artery model.* J Vasc Interv Radiol, 2001. **12**(3): p. 351-358.
91. Peeters, P., et al., *Preliminary results after application of absorbable metal stents in patients with critical limb ischemia.* J Endovasc Ther, 2005. **12**(1): p. 1-5.
92. Erbel, R., et al., *Temporary scaffolding of coronary arteries with bioabsorbable magnesium stents: a prospective, non-randomised multicentre trial.* Lancet, 2007. **369**(9576): p. 1869-75.
93. Zartner, P., et al., *First biodegradable metal stent in a child with congenital heart disease: evaluation of macro and histopathology.* Catheter Cardiovasc Interv, 2007. **69**(3): p. 443-6.
94. Zartner, P., et al., *First successful implantation of a biodegradable metal stent into the left pulmonary artery of a preterm baby.* Catheter Cardiovasc Interv, 2005. **66**(4): p. 590-4.
95. Schranz, D., et al., *Bioabsorbable metal stents for percutaneous treatment of critical recoarctation of the aorta in a newborn.* Catheter Cardiovasc Interv, 2006. **67**(5): p. 671-3.
96. Vogt, F., et al., *Long-term assessment of a novel biodegradable paclitaxel-eluting coronary polylactide stent.* Eur Heart J, 2004. **25**(15): p. 1330-1340.
97. Schultz, R., *REVA Medical, Inc. Bioresorbable technology*, in *CRT*. 2006: Washington, DC.
98. Edwards, B.S., et al., *Morphologic changes in the pulmonary-arteries after percutaneous balloon angioplasty for pulmonary arterial-stenosis.* Circulation, 1985. **71**(2): p. 195-201.
99. Edelman, E.R. and C. Rogers, *Hoop dreams. Stents without restenosis.* Circulation, 1996. **94**(6): p. 1199-202.
100. Farb, A., et al., *Pathology of acute and chronic coronary stenting in humans.* Circulation, 1999. **99**(1): p. 44-52.
101. Garasic, J.M., et al., *Stent and artery geometry determine intimal thickening independent of arterial injury.* Circulation, 2000. **101**(7): p. 812-8.
102. Barth, K.H., et al., *Paired comparison of vascular wall reactions to Palmaz stents, Strecker tantalum stents, and Wallstents in canine iliac and femoral arteries.* Circulation, 1996. **93**(12): p. 2161-9.
103. Ormiston, J.A., M.W.I. Webster, and P.N. Ruygrok, *Stent strut thickness and restenosis.* Circulation, 2002. **105**(2): p. E12-E12.
104. Kastrati, A., et al., *Intracoronary stenting and angiographic results: strut thickness effect on restenosis outcome (ISAR-STEREO) trial.* Circulation, 2001. **103**(23): p. 2816-21.

105. Barth, K.H., et al., *Flexible tantalum stents implanted in aortas and iliac arteries: effects in normal canines.* Radiology, 1990. **175**(1): p. 91-6.

106. Ohkubo, M., et al., *Histological findings after angioplasty using conventional balloon, radiofrequency thermal balloon, and stent for experimental aortic coarctation.* Pediatr Int, 2004. **46**(1): p. 39-47.

107. Ino, T. and M. Ohkubo, *Dilation mechanism, causes of restenosis and stenting in balloon coarctation angioplasty.* Acta Paediatr, 1997. **86**(4): p. 367-71.

108. Cook, R.D., et al., eds. *Concepts and applications of finite element analysis*. 2002, Wiley: New York. 719.

109. *Ansys Inc., Theory reference*. Ansys release 9.0 January 27, 2009]; Available from: http://www1.ansys.com/customer/content/documentation/90/ansys/a_thry90.pdf.

110. Fung, Y.C. and P. Tong, eds. *Classical and computational solid mechanics*. Advanced series in engineering science. Vol. 1. 2001, World Scientific Publishing: Singapore. 930.

111. *Plasticity*. January 29, 2008]; Available from: http://www.aaue.dk/bm/ansys/plast.pdf.

112. Chakrabarty, J., ed. *Applied plasticity*. Mechanical engineering series. 2000, Springer: New York. 682.

113. Kaliszky, S., ed. *Plasticity : theory and engineering applications*. Studies in applied mechanics. 1989, Elsevier: New York. 505.

114. *Material Nonlinearity*. January 29, 2009]; Available from: http://www.aaue.dk/bm/ansys/FEM-nonlinear-material-I.pdf.

115. Crisfield, M.A., ed. *Non-linear finite element analysis of solids and structures*. Adv Topics. Vol. 2. 1997. 508.

116. Hughes, T.J.R. and E. Carnoy, *Nonlinear finite element shell formulation accounting for large membrane strains.* Comput Methods Appl Mech Eng, 1983. **39**: p. 69-82.

117. De Beule, M., et al., *Realistic finite element-based stent design: The impact of balloon folding.* J Biomech, 2008. **41**(2): p. 383-389.

118. Park, W.-P., et al., *Evaluation of stent performances using FEA considering a realistic balloon expansion.* Inter J of Math Phys Eng Sc, 2008. **2**(2): p. 103-108.

119. Auricchio, F., M.D. Loreto, and E. Sacco, *Finite-element analysis of a stenotic artery revascularization through a stent insertion.* Comp Meth Biomech Biomed Eng, 2001. **4**(3): p. 249-263.

120. Wang, Y., H. Yi, and Z. Ni, *Computational biomechanics and experimental verification of vascular stent* Lecture Notes in Computer Science. Vol. 3801. 2005, Xi'an, China: Springer Berlin / Heidelberg.

121. Shen, X., H. Yi, and Z. Ni, *Effects of stent design parameters on radial force of stent*, in *the 2nd international conference on bioinformatics and biomedical engineering*. 2008: Nanjing. p. 1712-1716.

122. Migliavacca, F., et al., *A predictive study of the mechanical behaviour of coronary stents by computer modelling.* Med Eng & Phys, 2005. **27**(1): p. 13-18.

123. Chua, S.N.D., B.J. Mac Donald, and M.S.J. Hashmi, *Finite-element simulation of stent expansion.* J Mat Process Tech, 2002. **120**(1-3): p. 335-340.

124. Chua, S.N.D., B.J. Mac Donald, and M.S.J. Hashmi, *Finite element simulation of stent and balloon interaction.* J Mat Process Tech, 2003. **143**: p. 591-597.

125. Chua, S.N.D., B.J. MacDonald, and M.S.J. Hashmi, *Finite element simulation of slotted tube (stent) with the presence of plaque and artery by balloon expansion.* J Mat Process Tech, 2004. **155-56**: p. 1772-1779.

126. Chua, S.N.D., B.J. MacDonald, and M.S.J. Hashmi, *Effects of varying slotted tube (stent) geometry on its expansion behaviour using finite element method.* J Mat Process Tech, 2004. **155-56**: p. 1764-1771.

127. *What is an Atrial Septal Defect?* August 27, 2009]; Available from: http://kidshealth.org/parent/medical/heart/asd.html.

128. *What is Tetralogy of Fallot*. August 27, 2009]; Available from: http://www.nhlbi.nih.gov/health/dci/Diseases/tof/tof_what.html.

Glossary

- Atrial spetal defect: is congenital heart defect in which there is abnormal opening in the wall between the atria (upper two chambers of the heart)[127].
- Blalock-Taussig shunts: is a surgical procedure in which a detour (shunt) is created from the aorta to pulmonary artery to direct oxygen poor blood to the lungs.
- Pulmonary artery atresia: is a congenital heart defect in which the orifice of the pulmonary valve is underdeveloped resulting in blood outflow obstruction from the heart to the lungs.
- Pulmonary hypertension: is an increase in the blood pressure in the pulmonary circulation.
- Pulmonary oedema is fluid accumulation in the lungs which may cause respiratory failure.
- Tetralogy of fallot: is a congenital heart defect that regroups four main defects, a ventricular septal defect, pulmonary stenosis, right ventricular hypertrophy and an overriding aorta. [128]
    - Ventricular septal defect (VSD): is a congenital heart defect in which the septum, the thin wall separating the two ventricles has a hole, allowing the oxygen-rich and oxygen-poor bloods to mix.
    - Pulmonary stenosis: is the narrowing at or just below the pulmonary valve.
    - Right ventricular hypertrophy: is the thickening of the right ventricle as a result of pumping harder to allow blood through a narrowed pulmonary valve.
    - Overriding aorta: the aorta is positioned over a VSD instead of over the left ventricle. As a result, the aorta receives poor oxygen blood from the right ventricle.
- Truncus arteriosus is a rare congenital defect in which the aorta and pulmonary artery fail to separate upon embryonic development. This results in a single blood vessel arising from both ventricles instead of two.
- Ventilation-perfusion mismatch is a mismatch between the air in the lungs (ventilation) and the blood reaching to the lungs (perfusion)

Appendix A - Detailed drawings

All dimensions are in mm

1) Straight backbone stent

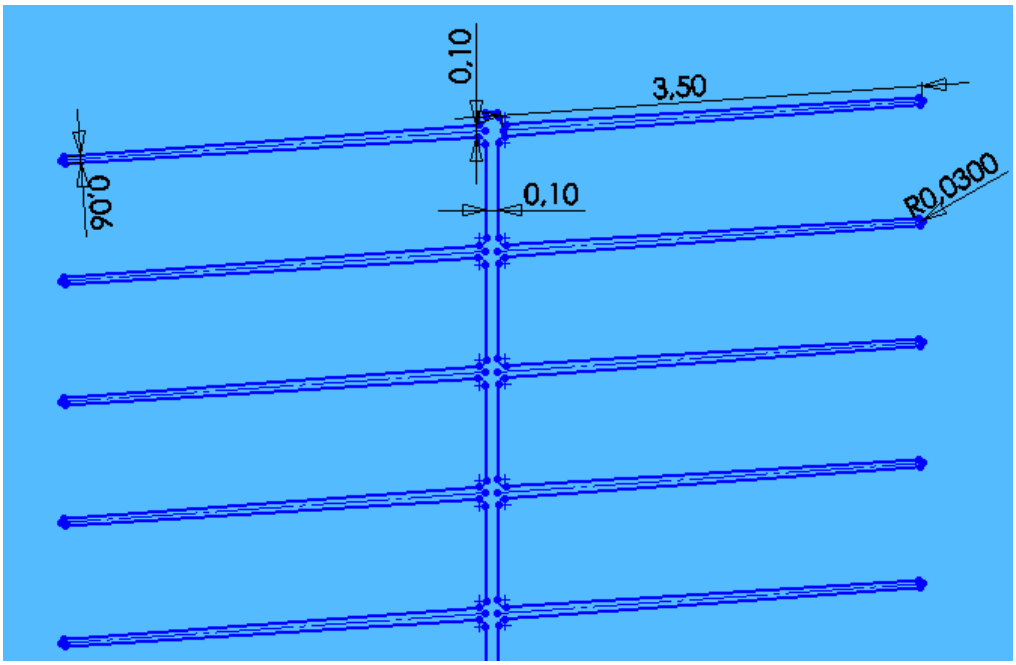

Figure A.1: Principal dimensions of of the straight backbone stent

Note that this stent has not been manufactured and is presented here only for comparison with the helical stent. As mentioned earlier, the backbone is straight and the struts are drawn at a slight angle from the vertical to have overlapping ribs.

2) Helical backbone stent

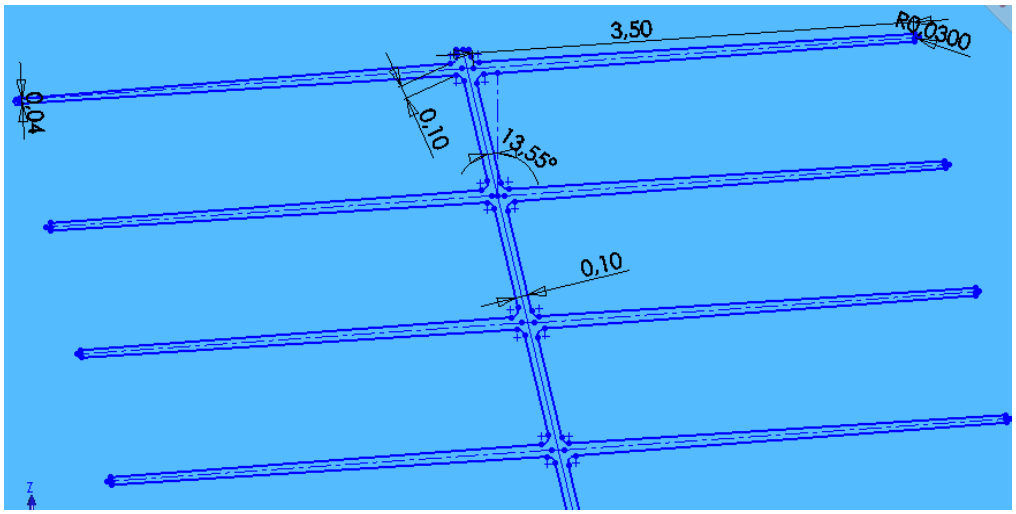

Figure A.2: Principal dimensions of the helical backbone stent

Helical stent length is 19.55mm

Stent outer diameter is 1.50 mm

In the helical backbone design, the backbone itself is drawn at an angle: The larger the angle, the larger the pitch of the helix.

3) Generation 2 stent : Alternating backbone

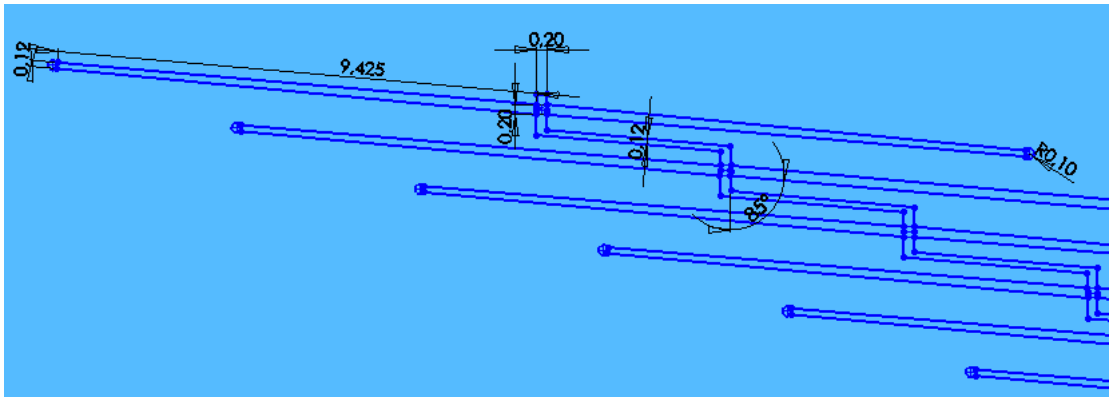

Figure A.3: Principal dimensions of the alternating backbone stent

The length of the stent is 18.55mm

Stent outer diameter is 2.30 mm

The alternating backbone stent is drawn as vertical backbone pieces, having the link and struts parallel to each other and forming an angle with the horizontal. (Figure A.3)

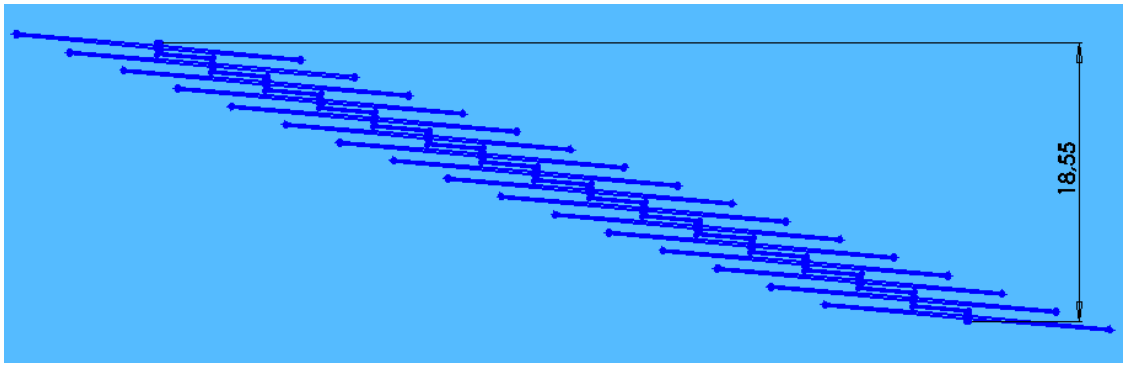

Figure A.4: 2-D drawing of alternating backbone stent

4) Generation 3 stent: Alternating backbone, version 2

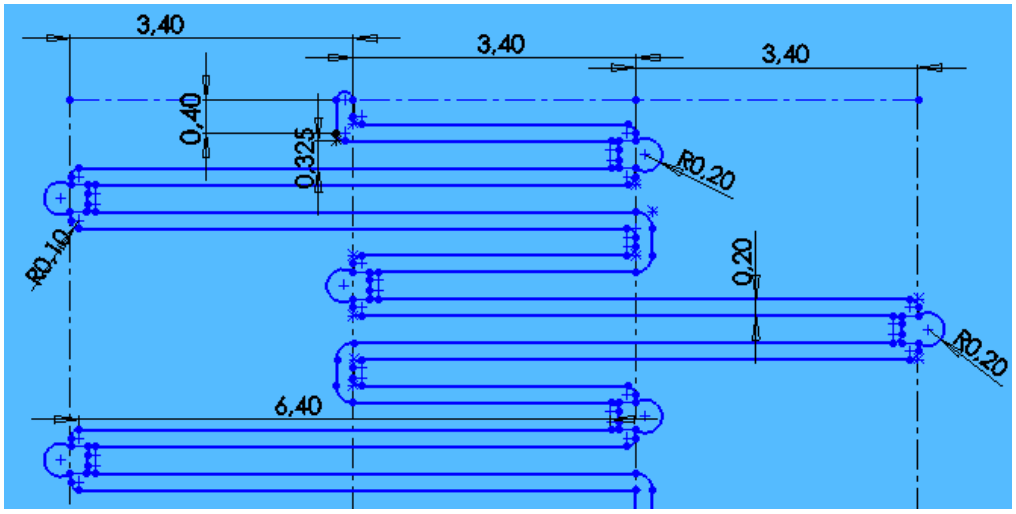

Figure A.5: Principal dimensions of the alternating backbone stent, version 2

The stent length is 22.33 mm

Stent outer diameter is 2.30 mm

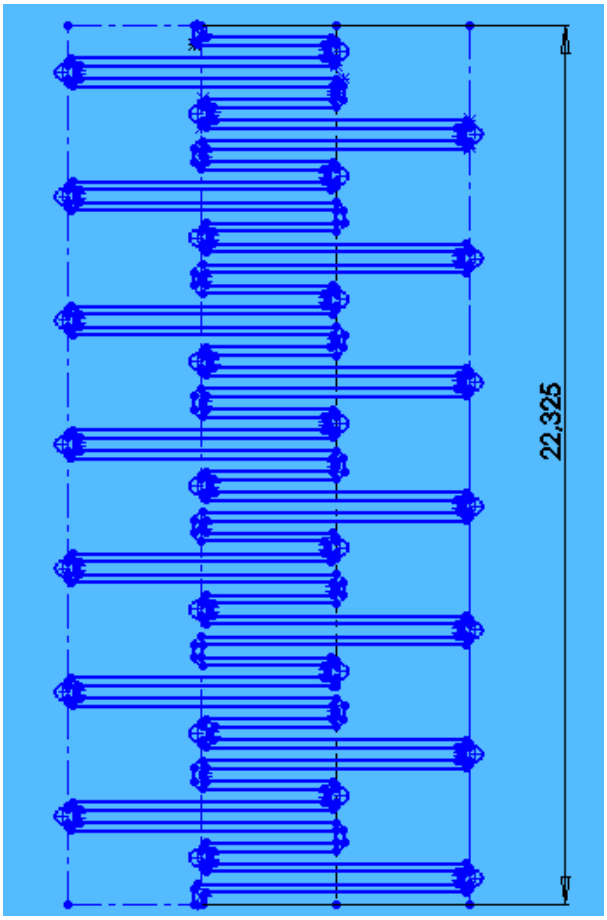

Figure A.6: 2-D drawing of alternating backbone stent, version 2

Appendix B: Sample Calculations for Test Data

B.1) Measuring Stent Lengths

Initial and final stent lengths are used to calculate foreshortening percentage of the stent. Using Adobe Photoshop, guide lines are used to measure in pixels a reference value of 10 mm and the stent length.

Figure B.1 below shows that 10mm is 483pixels. Similarly, the stent length is measured to 1018 pixels. Using a simple rule of three, the actual length of the stent is (1018×10/483)= 21.07mm

Taking three different pictures, the same procedure has been followed each time to measure the stent length. Next, the average of these three values is calculated.

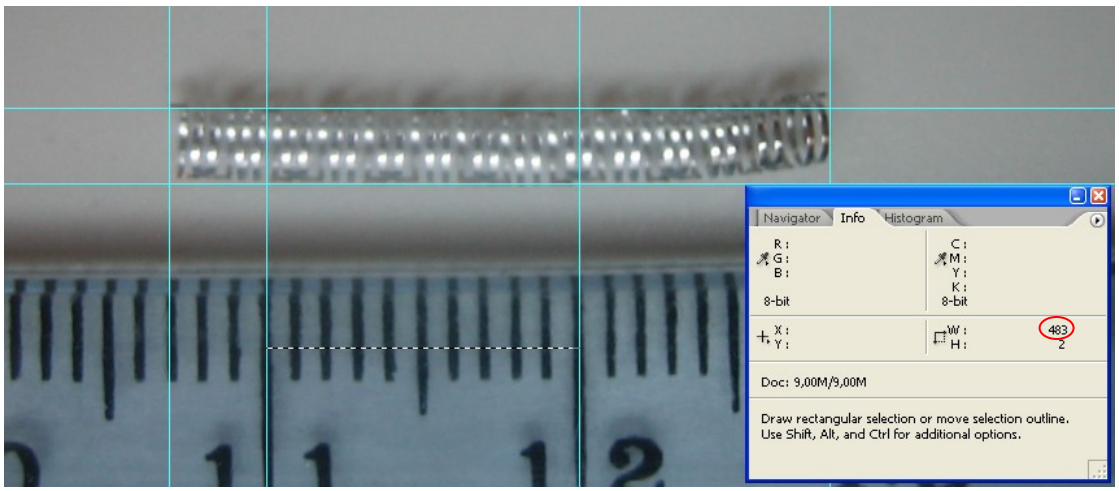

Figure B.1: Measuring initial stent length

The same procedure is applied to measure stent length after expansion. (Figure B.2)

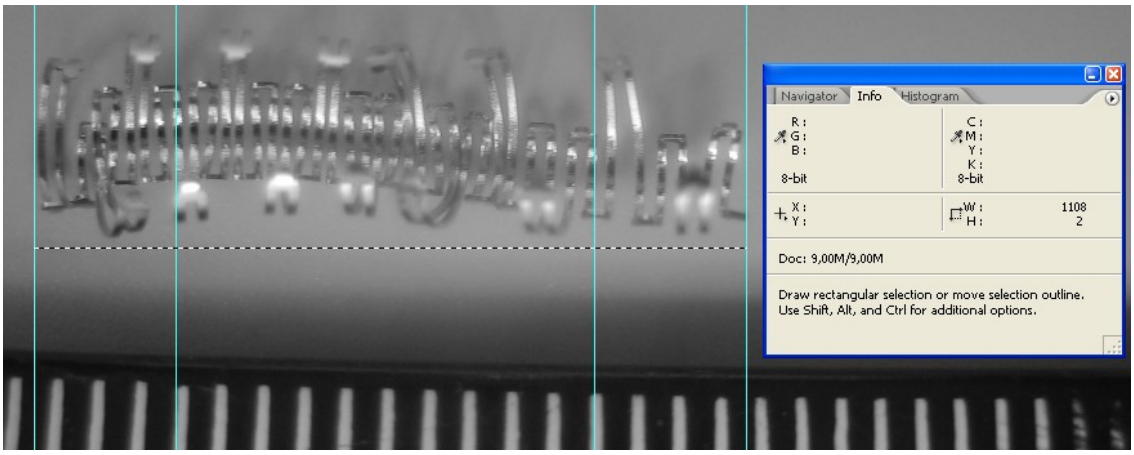

Figure B.2: Measuring final stent length

Finally stent foreshortening is calculated:

$$\%FS = \frac{L_i - L_f}{L_i} \times 100$$

B.2) Measuring Stent Diameter

To calculate recoil, stent diameter when balloon is fully inflated (here 5mm) and stent diameter after balloon removal are needed. Using the same procedure for the length, the stent diameter is measured. Here, the small rigid tube is which the stent is stored has been used as the reference value. Its outer diameter has been measured using a digital vernier caliper. Again, each dimension is measured at least three times using three different pictures. Finally, using the average value, recoil can be calculated:

$$\%recoil = \frac{R_{Inflated} - R_{Deflated}}{R_{Inflated}} \times 100$$

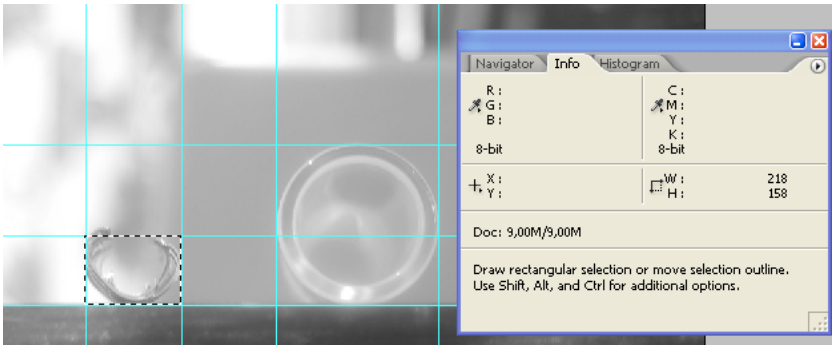

Figure B.3: Measuring final stent diameter